REACTIVE BALANCE STRATEGY IDENTIFICATION USING MOTION CAPTURE AND UNSUPERVISED CLUSTERING

WERAPAT LAPAWONG

MASTER OF SCIENCE
IN
DIGITAL TRANSFORMATION TECHNOLOGY

SCHOOL OF APPLIED DIGITAL TECHNOLOGY
MAE FAH LUANG UNIVERSITY
2025

REACTIVE BALANCE STRATEGY IDENTIFICATION USING MOTION CAPTURE AND UNSUPERVISED CLUSTERING

WERAPAT LAPAWONG

THIS THESIS IS A PARTIAL FULFILLMENT OF THE REQUIREMENTS FOR THE DEGREE OF MASTER OF SCIENCE IN DIGITAL TRANSFORMATION TECHNOLOGY

SCHOOL OF APPLIED DIGITAL TECHNOLOGY
MAE FAH LUANG UNIVERSITY
2025

THESIS APPROVAL

MAE FAH LUANG UNIVERSITY

FOR

MASTER OF SCIENCE

IN

DIGITAL TRANSFORMATION TECHNOLOGY

Thesis Title: Reactive Balance Strategy Identification Using Motion Capture and Unsupervised Clustering

Author: Werapat Lapawong

Examination Committee:

Associate Professor Phasit Charoenkwan, Ph. D.	Chairperson
Assistant Professor Worasak Rueangsirarak, Ph. D.	Member
Assistant Professor Surapong Uttama, Ph. D.	Member
Patcharaporn Panwong, Ph. D.	Member
Assistant Professor Sujitra Arwatchananukul, Ph. D.	Member

Advisors:

....Advisor

(Assistant Professor Worasak Rueangsirarak, Ph. D.)

....Co-Advisor

(Assistant Professor Surapong Uttama, Ph. D.)

Dean:

....

(Associate Professor Nacha Chondamrongkul, Ph. D.)

ACKNOWLEDGEMENTS

I would like to express my heartfelt gratitude to everyone who contributed to the successful completion of this research. First and foremost, I am deeply thankful to my advisor for their invaluable guidance and insightful feedback throughout this journey. Their expertise and dedication have been instrumental in shaping this work.

I am also grateful to the School of Applied Digital Technology, Mae Fah Luang University, for providing the necessary resources and support, which greatly facilitated this research. Special thanks to my colleagues and peers, who offered helpful suggestions, constructive criticism, and moral support during challenging times.

Lastly, I extend my deepest appreciation to my family and friends for their unwavering encouragement and understanding, which provided me with the strength and motivation to achieve my goals. This work would not have been possible without their support.

This research is supported by the Computer and Communication Engineering for Capacity Building Research Center, Mae Fah Luang University, Chiang Rai, Thailand, as part of the Erasmus+ "DigiHealth-Asia (2021-2024)" project under grant agreement no. 619193-EPP-1-2020-1-BE-EPPKA2-CBHE-JP. This work was also supported by a graduate research grant and a publication grant for ECTI DAMT & NCON 2025 from Mae Fah Luang University. The research was approved by the Mae Fah Luang Ethics Committee on Human Research, protocol no. EC 24225-13. The authors would also like to thank Dr. Haruthai Petviset, Dr. Sasima Pakulanon, and the faculty members of the School of Health Science, MFU, for their kind assistance.

The authors would like to thank our advisor for their guidance throughout this work, the School of Applied Digital Technology, Mae Fah Luang University, for their kind assistance and resources, and our families and friends for their unwavering support.

Werapat Lapawong

Thesis Title Reactive Balance Strategy Identification Using Motion Capture and Unsupervised Clustering

Author Werapat Lapawong

Degree Master of Science (Digital Transformation Technology)

Advisor Assistant Professor Worasak Rueangsirarak, Ph. D.

Co-Advisor Assistant Professor Surapong Uttama, Ph. D.

ABSTRACT

Balance is maintained through the continuous integration of visual, vestibular, and somatosensory inputs, translated into coordinated joint movements across the lower limb. Traditional balance assessments rely on subjective clinical observation, which limits the ability to detect complex, multi-joint strategies and hidden postural patterns. This thesis proposes an objective, data-driven framework integrating motion capture technology with unsupervised machine learning to identify balance strategies in both adult and pediatric populations.

The research was conducted in two phases. In Phase 1, the framework was developed and validated using the publicly available KINECAL adult dataset from PhysioNet. Three clustering algorithms — Agglomerative Hierarchical, Gaussian Mixture Model, and K-Means — were applied to lower-limb joint angle data, identifying three postural archetypes: Good Balance, Slight Unbalance, and Poor Balance. K-Means achieved the best performance at k=3, confirmed by the Elbow Method and Silhouette Score.

Continuously, the research was scoped down to explore the hidden balance strategies in children who experienced the Chronic Ankle Instability within the past year. In Phase 2, the framework was extended to 44 children aged 7 to 13 years-old performing the m-CTSIB under four sensory conditions, using the Xsens 17-sensor IMU system, underwent rigorous normalization and multicollinearity mitigation before being processed through four clustering algorithms: K-means, Spectral, BIRCH, and Hierarchical. The optimal four-cluster solution was validated through internal clustering metrics and PCA visualizations. Our analysis successfully delineated our

condition-specific postural archetypes: Mixed Strategy (Hip-Ankle), Ankle-Knee Strategy, and Atypical/Divergent patterns — each varying in joint amplitude and directional dominance across sensory conditions. Notably, the results revealed a sensory-dependent shift in motor control logic; while participants favored a localized Ankle Strategy during baseline and visual-deprivation tasks on stable surfaces, the removal of somatosensory cues forced a strategic shift toward a Mixed Strategy (Hip-Ankle). In the most demanding scenarios—where both visual and somatosensory inputs were compromised—the majority of children transitioned to a complex Integrated Strategy, necessitating synchronized Hip, Knee, and Ankle adjustments to maintain stability. Furthermore, the model also identified rare, atypical clusters characterized by divergent joint movement patterns — including opposite-directional responses and extreme distal amplitudes — that remain largely invisible to manual clinical observation.

To evaluate the quality and validity of clusters, this thesis proposed the new set of input features extracted from three rotational degrees of freedom (DoF) along with their joint descriptions. Cluster interpretations were further characterized through a plane-specific kinematic analysis — decomposing joint behavior across the sagittal (flexion/extension), frontal (abduction/adduction), and transverse (internal/external rotation) planes — consistent with ISB-recommended tri-planar reporting conventions. Each feature was further processed into three proposed temporal formats which are Discrete 5-second intervals (D5I), Segmented 5-second averages (S5A), and Overall trial mean (OTM). The metrics i.e. Silhouette Coefficient (SC), Calinski-Harabasz Index (CH), and Davies-Bouldin Index (DB) were used to confirm that the best clustering algorithm to identify the balance strategies in human are vary depending on different clinical scenarios.

Collectively, these findings demonstrate the testing of four different scenarios show that FiSEOTL reveals the majority of the population uses the Mixed Strategy (Hip-Ankle) by resulting of BIRCH clustering algorithm with the SC=0.420, CH=29.677, DB=0.578; while FiSECTL and FoSEOTL reveal the majority of the population use the Ankle-Knee Strategy by resulting of Spectral clustering algorithm with the SC=0.548, CH=22.759, DB=0.448 and Hierarchical Clustering with the SC=0.404, CH=28.940, DB=0.663 respectively; and the FoSECTL reveals the majority

of the population uses the Mixed Strategy (Hip, Knee, Ankle) by resulting of K-Means clustering algorithm with the SC=0.416, CH=33.812, DB=0.720.

Therefore, this thesis demonstrates that unsupervised clustering applied to motion capture data provides objective and clinically meaningful insights into balance strategy use that traditional observation-based assessment cannot offer.

Keywords: Balance Strategy, Motion Capture, Unsupervised Clustering, m-CTSIB Postural Control

TABLE OF CONTENTS

TABLE OF CONTENTS

LIST OF TABLES

LIST OF FIGURES

CHAPTER 1

INTRODUCTION

1.1 Background and Problem Identification

Maintaining balance is not a single fixed action. It is a continuous process in which the human body integrates information from three sensory systems — visual, vestibular, and somatosensory — and translates that information into coordinated joint movements across the ankle, knee, and hip. Depending on the conditions, individuals naturally adopt different strategies These strategies, and the transitions between them, form the foundation of postural control.

Understanding which balance strategy a person uses — and whether it is appropriate for the level of sensory challenge — is an important goal of clinical balance assessment. In practice, tests such as the Clinical Test of Sensory Interaction on Balance (CTSIB) and its modified version (m-CTSIB) are widely used to evaluate postural stability by systematically manipulating sensory conditions. However, these tests share a critical limitation: the results depend on the clinician's subjective interpretation of what they can observe. A trained assessor can note whether a patient sways or shifts weight but cannot reliably determine which joints are driving that response, or whether multiple strategies are being used at the same time (Gait & Posture, 2025).

This limitation becomes more significant when considering the complexity of real human movement data. When joint angles are recorded at high frequency using motion capture or wearable sensor systems, a single 30-second trial can produce thousands of data points across dozens of kinematic features. No clinician can meaningfully interpret this volume of information through observation alone. As a result, complex balance patterns — particularly those involving simultaneous coordination of multiple joints — remain invisible in routine clinical practice.
Conventional clinical scoring has been shown to maybe fail to distinguish meaningful differences in joint-level behavior, even between patients with documented musculoskeletal conditions and healthy controls (PLOS Digital Health, 2023).

The problem is present across both adult and pediatric populations, but for different reasons. In adults, balance strategies are relatively stable but highly individual — some people predominantly use an ankle strategy, others a hip strategy, and many use mixed combinations. Current clinical assessments rely heavily on in-person evaluations and subjective interpretation, limiting their ability to scale and provide objective insight into these individual differences (Gait & Posture, 2025). Without an objective framework, clinicians have no reliable way to determine which specific joints are failing to contribute appropriately to postural stability, or whether a patient's strategy is changing over time.

In children, the challenge is even greater. Postural control in children aged 7- to 10-years-old is still actively developing. Research has confirmed that postural stability in children matures through a process of more selective and refined re-weighting of proprioceptive inputs, particularly in the absence of visual input, and that this development continues well into the early school years (Journal of NeuroEngineering and Rehabilitation, 2005). This means that children in this age group may display a wide range of balance strategies — some appropriate for their developmental stage, others indicative of underlying motor planning difficulties — that are not distinguishable through standard observational scoring. Specialized assessment tools are needed to identify specific deficient postural control systems in children, particularly those with developmental coordination difficulties (Archives of Physical Medicine and Rehabilitation, 2025).

Postural instability represents a critical health challenge across all age groups, leading to severe clinical outcomes such as an increased risk of falls, peripheral neuropathy, Parkinson’s disease, and Developmental Coordination Disorder (DCD). Beyond physical injuries, balance impairments also trigger significant psychological consequences, including a persistent fear of falling (FoF) and chronic musculoskeletal pain.

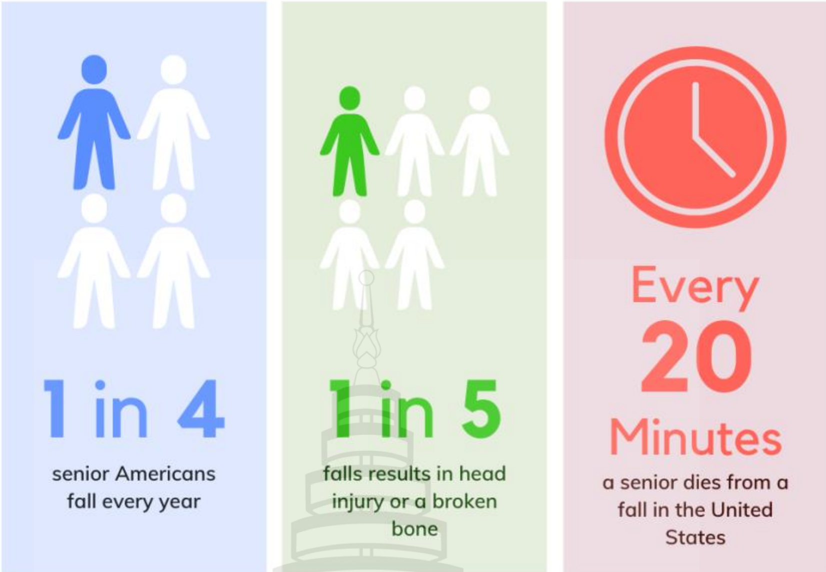

Source Royal Oaks Home Care (n.d.)

Figure 1.1 Statistics on falls

The global statistics on fall risks are particularly alarming. According to the World Health Organization (WHO), falls are the second leading cause of accidental death worldwide. Approximately 28-35% of individuals aged 65 and over experience at least one fall annually, a figure that rises to 32-42% for those over 70. Common injuries, as illustrated in Figure 1, range from fractures of the wrist, hip, and ankle to severe traumatic brain injuries. A specialized CDC report highlighted that 56,000 older adults are hospitalized annually due to fall-related head injuries, resulting in nearly 8,000 deaths (World Health Organization, 2007).

While childhood falls are often dismissed as a normal part of growth, they remain the leading cause of non-fatal injuries for those aged 0–19. In the United States alone, emergency departments treat over 2.8 million children annually for fall-related traumas (Rhode Island Department of Health). From an economic perspective, the burden is staggering; approximately \$50 billion is spent each year on medical expenses related to non-fatal falls. In long-term care facilities, the CDC reports between 100 and 200 falls per year, with the average cost per incident potentially exceeding \$17,000. (Secure Safety Solutions, 2020).

Developmental Coordination Disorder (DCD) is a common neuromotor condition affecting approximately 5%–6% of school-aged children (Harris et al., 2015). It is often under-recognized, with prevalence estimates ranging from 2% to 20% across studies, although 5%–6% remains the most frequently cited figure (Tamplain et al., 2024).

Fear of falling (FoF) affects nearly 50% of older adults worldwide, causing problems in daily life and reducing quality of life, leading to decreased physical function and an increased risk of falls (MacKay et al., 2021).

Finally, the psychological impact cannot be overlooked. The WHO reports that approximately 1.71 billion people globally live with musculoskeletal conditions, which are a major cause of disability worldwide, affecting over 50% of adults and increasing to 65-85% of older adults (Secure Safety Solutions, 2020).

Current clinical balance tests are commonly used to evaluate postural stability and fall risk in individuals, particularly the elderly there are 4 common balance assessment tests including:

1. Timed Up and Go (TUG) Measures mobility and balance by timing how long it takes to rise from a chair, walk a short distance, and return disadvantages Unable to predict falls in the community, Test-retest user error can be high, and Turning is only assessed in the patient's preferred direction (Barry et al., 2014; Shumway-Cook et al., 2000).

2. The Berg Balance Scale (BBS) evaluates a patient's balance through 14 tasks rated on a 5-point scale, taking approximately 20 minutes (Berg et al., 1992). While effective for assessing static and dynamic balance, it lacks gait assessment, limiting its comprehensiveness. A further limitation is that BBS scores in patients with spinal cord injury do not reliably predict fall risk (Wirz et al., 2010).

3. The Functional Reach Test (FRT) has proven to be a valuable clinical tool in this context (Duncan et al., 1990). It evaluates an individual's stability by assessing their ability to reach forward without losing balance. This test is complex, requiring coordination of multiple joints, including the legs, hips, and spine (Jonsson et al., 2003).

4. The Clinical Test of Sensory Interaction in Balance (CTSIB) is a clinical version of the Sensory Organization Test, developed to assess sensory contributions to

postural control by having the patient stand with hands at the sides, feet together, while performing six sensory conditions (Shumway-Cook & Horak, 1986).

The Clinical Test of Sensory Integration and Balance (CTSIB) have several advantages and disadvantages. Among its pros, the test is easy to implement, requiring minimal equipment like foam pads, a stopwatch, and blindfolds. It is versatile across age groups, being useful not only for older adults and individuals with balanced impairments but also for pediatric and athletic populations, providing valuable insights into sensory integration and postural control. Additionally, CTSIB is cost-effective, offering a low-cost alternative compared to advanced systems while maintaining its relevance for assessing sensory contributions to balance and in phase 2, we used CTSIB on children, called M-CTSIB. An additional device was added: a head-mounted dome specifically designed for M-CTSIB.

However, CTSIB also has its limitations. It can be time-consuming, as it involves conducting multiple tests under varying conditions, which may pose challenges in busy clinical settings. The controlled conditions used in CTSIB, such as foam surfaces and closed eyes, may fail to replicate the complexities of real-world environments, limiting
its applicability in those contexts. Furthermore, the test's reliability can be affected by inconsistent scoring methods across practitioners or settings, potentially influencing the accuracy of results.

Our research was conducted using the CTSIB method. The CTSIB test was developed by physical therapists ShumwayCook and Horak in 1986 to design a fall risk assessment for older adults. The test has evolved over the years to include four conditions, including static stability and dynamic stability using a foam board. CTSIB: The CTSIB test evaluates participants' ability to maintain balance under various sensory conditions.
Each participant performed the following four conditions:

1. Standing on a firm surface with eyes open
2. Standing on a firm surface with eyes closed
3. Standing on a foam surface with eyes open
4. Standing on a foam surface with eyes closed

To address the limitations of traditional balance assessment, this study proposes an objective, data-driven framework that integrates motion capture technology with unsupervised machine learning. Rather than relying on clinician observation, the proposed approach extracts kinematic features directly from joint motion data, then applying clustering algorithms to identify distinct postural patterns automatically.

The framework is structured into two phases. In the first phase, the methodology is developed and validated using a publicly available adult dataset collected via the Microsoft Kinect system under Clinical Test of Sensory Interaction on Balance (CTSIB) conditions. Joint angles at the ankle, knee, and hip are computed using the Law of Cosines, and three clustering algorithms — K-Means, Agglomerative, and Gaussian Mixture Model — are applied to classify balance quality into distinct groups. This phase establishes whether unsupervised machine learning can meaningfully differentiate balance strategies without pre-assigned labels.

In the second phase, the validated framework is extended to a primary pediatric dataset. Using a 17-sensor Xsens IMU system, kinematic data were recorded from 44 children aged 7- to 13-year-olds performing the modified CTSIB (m-CTSIB) under four sensory conditions. A more advanced pipeline is introduced, incorporating multi-scale temporal feature engineering and four clustering algorithms, to identify hidden balance strategy archetypes that are not observable through standard clinical assessment.

1.2 Research Objective

The primary goal of this study is to develop and apply an objective, unsupervised machine learning framework for identifying balance strategies from motion capture data. The specific objectives are:

1. To develop a data-driven balance assessment pipeline by integrating motion capture data with clustering techniques and validate it using publicly available adult kinematic data.

2. To explore hidden balance strategies in children with chronic ankle instability, primary kinematic data were extracted from a full-body Xsens IMU system.

3. To propose the generated features computed from rotational degrees of freedom (DoF), together with their joint descriptions, for the proposed temporal formats.

4. To apply and compare multiple unsupervised clustering algorithms for identifying distinct postural archetypes in the pediatric cohort using quantitative internal validation metrics and determining the most effective algorithm for each sensory condition.

1.3 Research Questions

In this study, four research questions were selected as follows:

1. Unsupervised machine learning algorithms applied to adult kinematic data from the CTSIB can objectively classify balance quality into distinct groups — such as Good Balance, Slight Unbalance, and Poor Balance — that correspond to meaningful differences in joint coordination patterns at the ankle, knee, and hip.

2. A data-driven clustering framework developed and validated on adult motion capture data can be successfully extended to a pediatric cohort with appropriate feature engineering and algorithm selection.

3. Unsupervised clustering applied to children's kinematic data from the m-CTSIB can identify hidden balance strategy archetypes — including mixed multi-joint strategies — that are not detectable through standard clinical observation.

The balance strategies employed by children will shift depending on the sensory condition, with more complex multi-joint strategies emerging as sensory difficulty increases from firm-eyes-open (FiSEOTL) to foam-eyes-closed (FoSECTL).

1.4 Scope of Study

This study is structured into two sequential phases. Phase 1 employs a secondary dataset — the KINECAL: Kinematic Measures for Assessing Balance Control dataset (Version 1.0.3), obtained from PhysioNet — to validate a data-driven framework for classifying adult balance strategies under Clinical Test of Sensory Interaction on Balance (CTSIB) conditions. Joint angle features at the ankle, knee, and hip are computed via the Law of Cosines and processed through three unsupervised clustering algorithms (Agglomerative Hierarchical, K-Means, and Gaussian Mixture Model), with clustering quality evaluated using the Silhouette Score.

Phase 2 applies the developed framework to primary data collected from 44 children aged 7–13 years-old (19 males, 25 females) at a single institution. Static balance movements were recorded across four m-CTSIB conditions — firm surface with eyes open, firm surface with eyes closed, foam surface with eyes open, and foam surface with eyes closed — each held for 30 seconds using 17 Xsens IMU sensors sampled at 60 Hz, yielding 316,800 data frames. Feature engineering extracted three rotational degrees of freedom (Abduction/Adduction, Internal/External Rotation, and Flexion/Extension or Dorsiflexion/Plantarflexion) from the hip, knee, and ankle joints across three temporal formats (Discrete 5-Second Intervals, segmented 5-Second Averages, and Overall Trial Mean), producing up to 54 features per participant. Dimensionality reduction via Pearson correlation (threshold $r > 0.90$) was applied before partitioning data using four clustering algorithms — K-Means, BIRCH, Spectral Clustering, and Hierarchical Clustering. The optimal number of clusters was determined by the Elbow Method, and cluster quality was validated using the Silhouette

Coefficient, Calinski-Harabasz Index, and Davies-Bouldin Score. This study is limited to lower-limb joints and does not address upper-body kinematics, dynamic balance tasks, or clinical diagnosis.

1.5 Preliminary Agreement

The following agreements and conditions apply to this research:

1. All data collection for Phase 2 was conducted in accordance with the research ethics protocol approved by the Mae Fah Luang Ethics Committee on Human Research, under Protocol No. EC 24225-13. Written informed consent was obtained from the parents or legal guardians of all child participants prior to data collection.

2. Phase 1 of this study uses a publicly available secondary dataset (KINECAL, PhysioNet Version 1.0.3). No additional data collection or ethics clearance was required for this phase.

3. The Xsens MVN system with 17 IMU sensors was used as the primary data collection instrument for Phase 2. Sensor calibration was performed according to the manufacturer's standard protocol before each recording session to ensure measurement accuracy and consistency across participants.

4. All participants in Phase 2 were required to perform the four m-CTSIB conditions in a standardized standing posture — feet together, arms at the sides — for 30 seconds per condition. Participants who lost balance before 30 seconds had their remaining kinematic values set to zero, as a standardized protocol for representing loss of balance.

5. The clustering results produced by this study are intended as descriptive postural archetypes based on kinematic data. They are not clinical diagnoses and should not be interpreted as such without further validation by qualified healthcare professionals.

6. All data were processed and analyzed using Python. The analysis environment and code are documented to ensure reproducibility.

1.6 Terminology Definition

The following terms are used throughout this study with the definitions given below

Table 1.1 Definition of Terms Used in This Study

Term	Definition as Used in This Study
Balance Strategy	A pattern of coordinated joint movement used by the body to maintain postural stability.
Postural Control	The ability of the body to maintain its center of mass within the base of support through the integration of visual, vestibular, and somatosensory inputs.
m-CTSIB	Modified Clinical Test of Sensory Interaction on Balance. A standardized protocol that evaluates postural stability under four conditions by systematically manipulating surface type (firm or foam) and visual input (eyes open or closed).
IMU	Inertial Measurement Unit. A wearable sensor that measures acceleration, angular velocity, and orientation
Kinematic Data	Measurements of joint angles and body segment movements over time, captured using motion capture technology.
Silhouette Coefficient (SC)	An internal clustering evaluation metric that measures how similar a data point is to its own cluster compared to other clusters. Values range from -1 to +1, with higher values indicating better-defined clusters.
Calinski-Harabasz Index (CH)	A clustering evaluation metric that measures the ratio of between-cluster dispersion to within-cluster dispersion. Higher values indicate denser and more well-separated clusters.
FoSECTL	Foam Surface, Eyes Closed, Two-Leg Standing.
FiSECTL	Firm Surface, Eyes Closed, Two-Leg Standing.
FoSEOTL	Foam Surface, Eyes Open, Two-Leg Standing.

Table 1.1 (continued)

Term	Definition as Used in This Study
FiSEOTL	Firm Surface, Eyes Open, Two-Leg Standing.
Davies-Bouldin Score (DB)	A clustering evaluation metric that measures the average similarity between each cluster and its most similar neighboring cluster. Lower values indicate more distinct, non-overlapping clusters.
D5I	Discrete 5-Second Interval. A temporal feature format in which joint angle values are sampled at fixed 5-second time points (t = 5, 10, 15, 20, 25, 30 seconds) within a 30-second trial. This format captures transient postural fluctuations.
S5A	Segmented 5-Second Average. A temporal feature format in which the mean joint angle is calculated within each consecutive 5-second window of a 30-second trial. This format captures short term postural stability trends while reducing high-frequency noise.
OTM	Overall Trial Mean. A temporal feature format in which the mean joint angle is calculated across the entire 30-second trial. This format represents the participant's global postural strategy for a given condition.
PCA	Principal Component Analysis. A dimensionality reduction technique used in this study to project high-dimensional kinematic features into a 2D space for visual inspection and cluster validation.

CHAPTER 2

LITERATURE REVIEW

2.1 Theoretical Background

2.1.1 Human Balance

Human balance is a fundamental aspect of physical stability and movement, relying on complex interactions between sensory inputs, motor responses, and environmental factors. Understanding balance is essential for assessing fall risks, improving rehabilitation strategies, and advancing healthcare technologies. Balance theories are broadly categorized into three key frameworks: Sensory Organization, Dynamic Systems, and the Systems Theory of Motor Control.

Sensory Organization: This theory focuses on how the body processes sensory input to maintain balance. It suggests that balance control is distinct from the sensory perception of balance itself. Through testing, we can observe various strategies the body uses to maintain stability, such as shifting weight or changing posture. These strategies become especially significant when assessing fall risk.

Dynamic Systems: This theory explores how the body adapts its movement patterns based on the surrounding environment and physical conditions. It helps explain how different balance strategies, such as ankle, hip, and stepping responses, are developed and utilized. This understanding is crucial for analyzing and classifying balance strategies, particularly when examining how individuals respond to unstable surfaces or challenging conditions.

Systems Theory of Motor Control: This theory examines how various body systems—such as the central nervous system, respiratory system, circulatory system, and musculoskeletal system—work together to produce purposeful movements. It emphasizes the importance of adaptive balance strategies (like ankle, hip, and stepping responses) in maintaining stability. In this research, this theory underpins the categorization of different balance strategies using motion capture data and machine learning techniques.

2.1.2 Human Balance Assessment

Balance refers to the ability to maintain the body’s center of gravity within its base of support during static or dynamic activities. It ensures stability and helps recovery from disturbances. Imbalance can result from various health conditions and is associated with symptoms like falls, dizziness, and vertigo, which affect a significant portion of the population. Falls are a major health concern due to their impact on quality of life and healthcare costs. Therefore, there must be a Balance Assessment, which is divided into 3 main types:

Traditional Balance Assessments include subjective methods like the Berg Balance Scale and the Functional Gait Assessment, but these often rely on clinician interpretation, which may affect reliability. Modern objective tools, such as force plates and motion capture systems, provide precise data but are less commonly used due to their cost and complexity. There remains a need for accessible, quantitative balance assessment tools.

Modern Balance Assessment methods have advanced significantly to provide more precise and objective measurements. At-home monitoring systems, including wearable sensors and smartphone applications, are particularly useful for individuals at high risk of falls. Unlike traditional assessments, which are often subjective, modern methods rely on sensor-based technology such as force plates, accelerometers, gyroscopes, and 3D motion capture systems. These devices are portable, cost-effective, and capable of evaluating balance and gain in real-world settings, making them accessible for clinical and personal use. This shift toward technology enhances both the accuracy and practicality of balance evaluations.

Dynamic Balance is the ability to maintain stability while moving or performing tasks like walking or reaching. This skill is essential for safely navigating surroundings and avoiding falls. Impaired dynamic balance can limit mobility and independence, affecting overall health. Exercises to improve dynamic balance typically focus on enhancing coordination and strengthening muscles involved in weight transfer. Common exercises include standing on one leg, stepping tasks, and reaching out with hands or feet to objects placed nearby.

2.1.3 Tri-planar kinematic analysis

To interpret cluster-level joint behavior, this study adopted a tri-planar kinematic analysis framework — a plane-specific approach consistent with ISB-recommended reporting conventions (Wu et al., 2002). Rather than treating joint angles as a single aggregate measure, movements were decomposed across three anatomical planes: the sagittal plane, which captures flexion and extension at the hip, knee, and ankle (dorsiflexion/plantarflexion); the frontal plane, which reflects abduction and adduction movements primarily at the hip and knee; and the transverse plane, which represents internal and external rotation across all three joints. This decomposition allows each cluster to be characterized not only by the magnitude of joint displacement, but also by which plane — and which joint — contributes most to the observed postural response.

2.1.4 Physical Performance Assessment

Physical performance assessment evaluates an individual's mobility, strength, and balance, providing crucial insights into functional abilities, particularly in older adults and individuals with mobility challenges. These assessments are essential in predicting fall risks, designing rehabilitation plans, and monitoring physical health. The theory encompasses various tools and techniques that focus on different aspects of physical performance, which can be broadly categorized into sensory interaction and balance tests, mobility and strength evaluations, and balance strategy assessments.

Clinical Test for Sensory Interaction and Balance (CTSIB) assess postural stability by testing sensory control of balance in six conditions involving a rigid surface and foam with a variety of visual and balance data. A modified CTSIB (m-CTSIB) was developed as a simple alternative that still maintains reliability and usability.

The CTSIB systematically manipulates visual (eyes open vs. closed) and surface somatosensory (firm vs. foam) inputs to assess how the central nervous system reweighs sensory information for postural control. Under these varying conditions, the lower limb serves as the primary biomechanical effector of upright stability, with the ankle, knee, and hip each contributing distinct but interdependent roles. The ankle represents the first line of defense under stable conditions, generating corrective torque through localized adjustments; as surface stability decreases, somatosensory feedback from ankle mechanoreceptors becomes unreliable, prompting greater reliance on hip-level control or coordinated multi-joint responses (Horak & Nashner, 1986). The knee, acting as an intermediate link, modulates load transfer when compensatory demands exceed single-joint capacity — and may over-function to compensate for deficiencies at either adjacent segment. Because balance is maintained through coordinated multi-segmental responses rather than isolated joint action, measuring joint angles simultaneously across the hip, knee, and ankle — and across the frontal, transverse, and sagittal planes — provides a direct kinematic representation of the postural strategy employed under each condition. Furthermore, the 30-second trial duration captures the temporal evolution of these strategies: the initial phase (5–10 s) typically reflects reactive stabilization characterized by ankle-dominant responses, while the middle-to-terminal phase (15–25 s) reveals compensatory shifts potentially attributable to sensory reweighting or neuromuscular fatigue — enabling differentiation between participants who maintain stable coordination and those who exhibit strategy breakdown over time (Westcott et al., 1997).

The Short Physical Performance Battery (SPPB) is a free, standardized tool developed by the National Institute on Aging (NIA) to measure balance, lower body strength, and mobility in adults over 65. It includes walking, sit-to-stand, and balance tests. Training videos and a mobile app are available for consistent administration.

The Timed Up and Go (TUG) test is a clinical tool used to assess basic functional mobility, particularly in older adults. The test measures the time it takes for a person to rise from a chair, walk three meters, turn around, walk back, and sit down again. A stopwatch is traditionally used for timing, but modern adaptations include wearable devices that provide detailed biomechanical analysis of movements. TUG is a simple and quick assessment of mobility and balance, often used to predict the risk of falls. It is particularly valuable for evaluating individuals with conditions like Parkinson's disease and stroke. However, it has limitations, such as sensitivity to user error and difficulty detecting nuanced mobility impairments in certain populations.

Balance Strategies are mechanisms the body uses to maintain stability and control posture while standing, walking, or responding to external disturbances. These strategies include anticipatory postural adjustments, which involve activating muscles in preparation for movements or external forces, and compensatory adjustments, which respond to unexpected balance disruptions. Such training can significantly reduce the risk of falls, especially in populations with mobility issues.

2.1.5 Parameters of Fall Risk and Balance Assessment

Balance and fall risk assessment is crucial, particularly in older adults, to prevent falls and related injuries. Key parameters such as postural sway, joint angles, and sensory-motor integration are critical to understanding balance control and identifying potential risks. These parameters can be following that happen around the body's center of gravity to maintain balance. It is your body's natural adaptation to changing stimuli. It may be noticeable or unnoticeable. Those with poor balance and coordination exhibit greater postural sway (Winter, 1995).

Efficient gait relies on adequate joint mobility, particularly in the hips, knees, and ankles. Limited range of motion due to injury or aging can disrupt stability and movement, affecting balance and performance (Pirker & Katzenschlager, 2017).

Dynamic Balance Control Dynamic balance ensures stability during movement, essential for walking, running, and directional changes. It depends on coordinated sensory and motor functions, making it critical for sports and reducing fall risks (Neptune & Vistamehr, 2019).

Sensory-Motor Integration This process allows the brain to turn sensory inputs into smooth motor actions. Neuroplasticity helps restore function after injuries, enhance motor control and adaptability (Shumway-Cook & Woollacott, 2017).

Development of Data-Driven Metrics for Balance Impairment and Fall Risk Assessment in Older Adults uses postural sway, gait parameters (speed, stride length and variability) as Key Parameters and Development of a Motion Capture System for Fall Risk Assessment uses joint angles, CoM dynamics, and gait variability as Key Parameters.

2.1.6 Decision Support System in Healthcare

The world is awash in data, yet much of its potential remains untapped. Properly harnessed, data can address significant challenges and drive advancements across various sectors. A Decision Support System (DSS) or decision support tool helps unlock this potential by aggregating relevant data from diverse internal and external sources, analyzing it, and transforming it into actionable insights. These insights empower stakeholders to make informed, strategic decisions. An effective DSS provides structured data through customizable reporting and analysis tools, making complex data more accessible and comprehensible. It allows leaders to quantify the impacts of potential choices, identify strengths and weaknesses, and uncover opportunities for improvement. By enhancing decision-making processes, DSS tools become critical in navigating today's data-driven world.

Decision support systems (DSS) play a vital role in healthcare, enabling professionals such as clinicians and hospital leaders to process and analyze vast amounts of data to inform critical decisions. These systems integrate information from a variety of internal and external sources, supporting clinical, financial, and operational functions within hospitals and health systems.

As the volume and complexity of healthcare data grows, DSS technology provides solutions to aggregate and analyze this information. By collating, calculating, and extrapolating relevant data, decision support systems allow healthcare organizations to quantify the impact of decisions across various departments. These systems transform raw data into actionable insights, helping stakeholders respond effectively to dynamic market conditions and optimize care delivery, resource management, and financial outcomes.

Types of Decision Support in Healthcare

The primary types of decision support in healthcare are:

1. Financial Decision Support: Healthcare financial DSS helps executives and managers optimize efficiency, control costs, and enhance revenue. These systems aggregate data from diverse sources to support budgeting, monitor productivity, and evaluate performance. By providing actionable insights, they enable hospitals to align operations with strategic goals and adapt to changing financial landscapes.

2. Clinical Decision Support: Clinical DSS assist caregivers at the bedside by offering real-time data to enhance diagnosis and treatment. These systems leverage electronic health records (EHRs) and other data sources to minimize adverse events and improve care quality. The primary objective is to increase the efficiency and accuracy of patient care.

3. Clinical Analytics: Focusing on organizational performance, clinical analytics compare a hospital's data to peer institutions, offering insights into costs, utilization, and outcomes. This broader approach enables healthcare leaders to reduce

care variations, improve coordination, and enhance workforce productivity. Unlike clinical DSS, which supports individual patient care, clinical analytics evaluates service lines and patient cohorts, driving systemic improvements in care delivery.

2.1.7 Artificial Intelligence Machine Learning Theory

Artificial Intelligence (AI) simulates human intelligence in machines, enabling tasks like natural language processing (NLP), speech recognition, and computer vision. Many AI claims involve existing technologies such as machine learning, which require specialized hardware, software, and programming languages like Python, R, or C++ (Russell & Norvig, 2021).

Machine Learning, a subset of artificial intelligence (AI), focuses on teaching computers to learn from data and improve over time without explicit programming. It trains algorithms to detect patterns, make predictions, and refine decisions based on large datasets (Bishop, 2006).

Machine Learning includes deep learning and neural networks, which are nested within AI's broader framework. While AI processes data to make decisions, ML allows systems to learn and adapt independently, enhancing performance as more data becomes available.

The technique we used in both research studies was Unsupervised Machine Learning.

Unsupervised Learning is a machine learning method where algorithms analyze and find patterns in unlabeled data, meaning the data lacks predefined outputs or categories. Unlike supervised learning, the focus is on uncovering hidden structures, patterns, or groupings without explicit guidance. This makes unsupervised learning valuable for tasks like data exploration, visualization, and dimensionality reduction. The two main types of unsupervised learning are

Clustering: Grouping similar data points into clusters based on shared characteristics. Examples include customer segmentation and anomaly detection. Here are some clustering algorithms:

1. K-Means Clustering algorithm
2. Hierarchical Clustering
3. Spectral Clustering
4. BIRCH Clustering

5. Gaussian Mixture Model

Association: Identifying relationships or associations within data, often used in market basket analysis to find products commonly purchased together. Here are some association learning algorithms:

1. Apriori Algorithm
2. Eclat
3. FP-growth Algorithm

2.1.8 Pattern Recognition in Machine Learning

Pattern Recognition in Machine Learning involves analyzing data to identify patterns and regularities, even in partially hidden or unfamiliar objects. It works by classifying and clustering data points using statistical insights derived from past data representations. This technique is applied to various data types, such as text, images, and sounds, and is a specialized form of machine learning aimed at efficient data matching and analysis.

2.1.9 Data Mining in Healthcare

Data mining and clustering techniques have become increasingly valuable in healthcare for uncovering patterns within complex clinical datasets. Sang et al. (2022) and Miyazawa et al. (2020) demonstrated that unsupervised clustering can identify distinct patient subgroups in metabolic and diabetic populations, revealing heterogeneity that conventional diagnosis overlooks. In the context of human movement, (McManus et al., 2022) developed data-driven metrics from IMU data to objectively quantify balance impairment and fall risk in older adults, while Halilaj et al. (2018) established methodological benchmarks for applying machine learning to biomechanical data — both providing a direct foundation for the data-driven balance assessment framework employed in this study.

2.1.10 Motion Capture

Motion capture (mo-cap) is a technology that records the movement of objects or people and transfers this data to a digital system. It enables the creation of realistic animations for virtual environments by capturing natural and intricate movements. The process involves tracking the motion of actors and mapping it onto 3D models, allowing these models to replicate captured actions.

Applications for Motion Capture

Motion capture is widely used in various fields:

1. Entertainment: In films, TV shows, and video games, it enhances animation by adding lifelike movement and expressions.

2. Healthcare and Sports: It aids in biomechanical analysis, rehabilitation, and performance optimization.

3. Military: Used for training simulations and equipment testing.

Types of Motion Capture

Optical Passive: Infrared cameras track retroreflective markers attached to the subject.

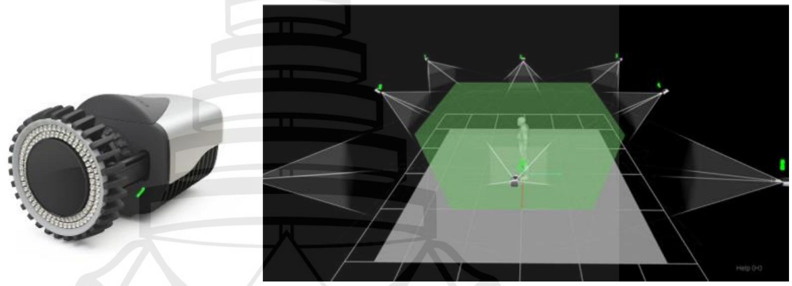

Source Assistive Robotics Center (n.d.)

Figure 2.1 Qualisys Motion Capture

Optical Active: Special cameras detect light emitted by LED markers on the subject.

Source Alhafis Hashim et al. (2024)

Figure 2.2 Example Optical Active (phasespace)

Video/Markerless: Uses software to track motion without physical markers.

Source Smeenk (2014)

Figure 2.3 Example Video/Markerless (Kinect)

Inertial: Involves wearable inertial sensors (IMUs) that transmit data wirelessly, often supplemented with cameras for localization.

Source Van Winkle (2014)

Figure 2.4 Example Inertial sensors (Neuron)

2.1.11 Xsens (inertial sensor motion capture device)

Xsens is a leading provider of 3D motion capture systems From the Swedish company Movella that use inertial sensor technology to track and analyze human movement with precision. These systems combine data from gyroscopes, accelerometers, and magnetometers to capture motion in real-time, enabling applications in biomechanics, animation, robotics, and sports science. The Xsens motion capture kit typically includes wearable sensors such as the MVN Link (wired) or MVN Awinda (wireless), along with MVN Analyze or MVN Animate software for data processing and visualization. Data is transmitted either wirelessly via radio signals or through high-speed wired connections, offering flexibility depending on the application. Xsens devices can measure various parameters, including joint angles, segment positions, velocities, accelerations, and center-of-mass tracking. These systems provide valuable insights for gait analysis, balance studies, and performance enhancement in clinical and research settings.

2.2 Related Works

2.2.1 Balance Strategy and Postural Control

Postural control is a fundamental aspect of human movement that relies on the integration of visual, vestibular, and somatosensory inputs to maintain stability (Horak, 2006). Research has shown that the strategies used to maintain balance change depending on sensory conditions and surface types. Westcott et al. reviewed assessment tools and theories for evaluating postural stability in children, forming an important theoretical basis for how balance strategies are tested in different conditions (Cuisinier et al., 2011). Cuisinier et al. studied children aged 7 to 11 years-old and found that they re-weight sensory inputs differently from adults during quiet standing, which shows that this age group is still developing their postural control strategies (Halilaj et al., 2018).

The reliability of balance assessment tools has also been studied. Van Gulick et al. tested the reliability of static and dynamic balance assessments using a pressure platform in clinical settings, pointing to the need for more consistent and objective measurement methods (Westcott et al., 1997). Blenkinsop et al. examined how balance control strategies are used in both disturbed and undisturbed standing conditions and found that mixed strategies become more prominent when balance demands increase (Blenkinsop et al., 2017). These studies confirm that balance strategy use is complex and cannot be fully captured by simple observation alone.

2.2.2 Motion Capture Technology

Motion capture technology is widely used for the objective measurement of human movement and balance. Marker-based optical systems such as Vicon are commonly used in life sciences and clinical research because of their high accuracy Scataglini et al., 2024). IMU-based systems are a wearable alternative that can be used outside the laboratory. (Al-Amri et al., 2018) that IMU systems provide reliable and valid measurements for clinical movement analysis and validated the Xsens IMU system for lower-body kinematics in dynamic movement tasks, supporting its use in postural analysis (Nijmeijer et al., 2023).

Markerless motion capture is another approach that allows balance assessment without attaching physical markers to the body (Scataglini et al., 2024). McManus et al. used IMU data to develop data-driven metrics for assessing balance impairment in older adults (Di Raimondo et al., 2022), while Museck et al. reviewed wearable sensor methods for estimating biomechanical characteristics while standing and walking (Museck et al., 2024). Alderink and Õunpuu also provided a comprehensive review of instrumented gait analysis and its clinical applications, further supporting the use of kinematic data in movement classification (Di Raimondo et al., 2022). Together, these studies show that motion capture technology, whether marker-based, wearable, or markerless, provides an objective foundation for balance research.

2.2.3 Machine Learning in Movement and Balance Classification

Machine learning has been increasingly used in human movement analysis to provide objective and scalable alternatives to clinical observation. best practices and common challenges in applying machine learning to human movement biomechanics, noting the importance of careful feature selection and validation (Halilaj et al., 2018). Zago et al. also discussed how machine learning approaches are growing in movement analysis for identifying patterns that are difficult to see through conventional assessment (Zago et al., 2021).

Several studies have applied machine learning specifically to balance and body imbalance classification. Gul et al. classified body imbalance and its intensity using electromyogram and ground reaction force data, showing that automated classification of postural instability is both practical and accurate (Gul et al., 2024), (Shen et al., 2020). Roshdibenam et al. showed that machine learning can predict fall risk in older adults using kinematics from the Timed Up and Go test (Roshdibenam et al., 2021), (Halvorson et al., 2022). Heritage also explored accelerometric machine learning techniques for human balance analysis, providing early evidence for data-driven approaches in postural stability research (Eltoukhy et al., 2017).

2.2.4 Clustering Techniques in Healthcare and Gait Analysis

Clustering is an unsupervised machine learning technique that has been applied in healthcare to find meaningful subgroups in complex data without needing pre-assigned labels. It has been used to identify patient segments, support disease subtyping, and improve patient management (Sang et al., 2022; Hoadley et al., 2018; Miyazawa et al., 2020). In movement and gait analysis, Dugan et al. used K-Means clustering to identify distinct kinematic foot types in children with cerebral palsy, showing that clustering can reveal clinically meaningful postural subtypes in a pediatric population (Gul et al., 2024). Russo et al. applied cluster analysis to Parkinson's disease gait data to identify movement phenotypes (Russo et al., 2023), and Ghanem studied dynamic time warping as a method for improving clustering accuracy on sequential data, which is directly relevant to temporal kinematic features used in balance analysis (Ghanem., 2013).

In balance strategy research specifically, Shen et al. used Numerical Model Predictive Control (N-MPC) to predict effective balance recovery strategies under various disturbances and measured mixed hip-ankle strategies in challenging conditions Ghanem, K. (2013). Atkeson and Stephens showed that multiple balance strategies can emerge from a single optimization criterion in humanoid robotic systems, providing evidence that balance behavior is inherently multi-strategy (Atkeson & Stephens, 2007).

Although these studies provide a strong foundation, most focus on supervised classification, single-strategy identification, or adult populations only. There is still a gap in using unsupervised clustering to identify the full range of balance strategy archetypes, including mixed and hidden patterns, in both adult and pediatric populations using motion capture data. This gap is the direct motivation for the present research.

2.3 Summary

The literature reviewed in this chapter covers three main areas that are directly relevant to this research: balance strategy and postural control, motion capture technology, and machine learning — particularly clustering techniques applied to human movement data.

From the review, it is clear that balance is not a single, fixed response but a continuous process of multi-joint coordination that changes depending on sensory conditions. Although clinical tests such as the CTSIB and m-CTSIB are widely used, they share a fundamental limitation — they rely on subjective observation, which cannot detect complex or mixed strategies occurring simultaneously across the hip, knee, and ankle. This limitation is present in both adults and children and becomes more significant when working with high-dimensional kinematic data that exceeds what any clinician can interpret by eye.

Motion capture technology, whether marker-based, IMU-based, or markerless, has been shown to provide objective and high-frequency measurement of joint kinematics that addresses this limitation. In particular, the Xsens IMU system has been validated for lower-limb kinematic analysis in clinical and dynamic movement settings, making it a suitable tool for collecting primary pediatric data in this study.

The review of machine learning methods shows that unsupervised clustering has been successfully applied to healthcare and gait analysis to identify meaningful subgroups in complex data without pre-assigned labels. However, most existing work focuses on supervised classification, single populations, or single strategies at a time. No prior study has applied unsupervised clustering to identify the full range of balance strategy archetypes — including mixed and hidden patterns — across both adult and pediatric populations using motion capture data.

Based on these gaps, this research proposes a two-phase, data-driven framework. In Phase 1, the framework is developed and validated using a publicly available adult dataset, applying three clustering algorithms to lower-limb joint angle data under CTSIB conditions to identify objective balance quality groups. In Phase 2, the validated framework is extended to 44 children aged 7 to 13 years-old performing the m-CTSIB, using a more advanced pipeline that incorporates multi-scale temporal feature engineering, correlation-based dimensionality reduction, and four clustering algorithms to identify hidden postural archetypes across four sensory conditions.

Together, these two phases aim to demonstrate that unsupervised machine learning applied to motion capture data can provide objective, scalable, and clinically meaningful insights into balance strategy use that traditional observation-based assessment cannot offer.

CHAPTER 3

METHODOLOGY

3.1 Research Overview

Our research is structured into two sequential phases, moving from framework validation using public datasets to primary data application in pediatric populations.

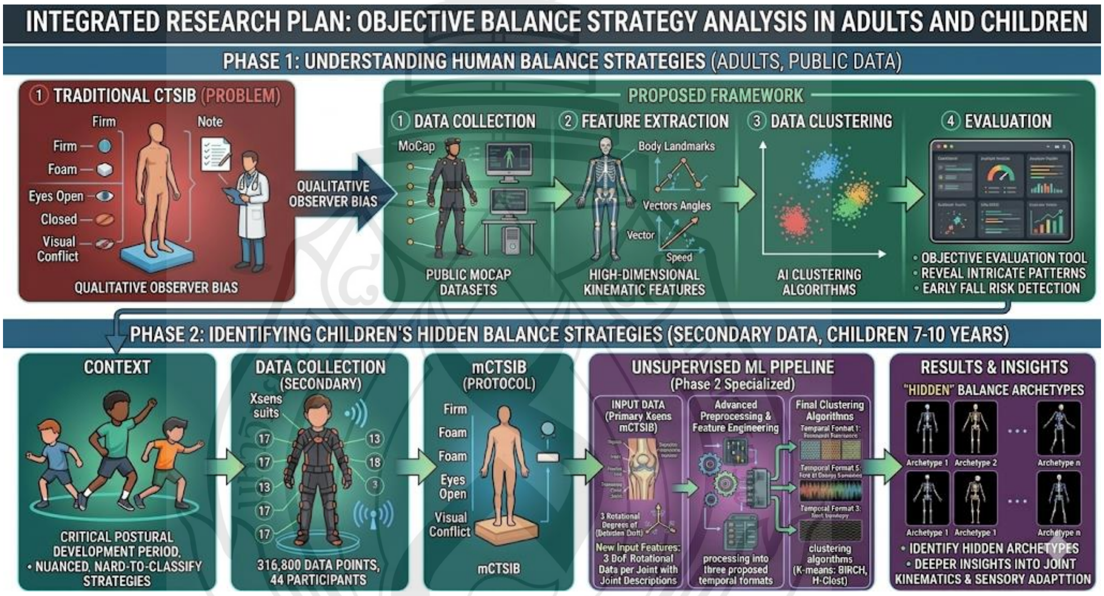

Figure 3.1 Research Overview Workflow

The overview of the proposed research can be distinguished into two phases. The 1st phase focuses on understanding human balance strategies through clustering of publicly available motion analysis data focuses on lower-limb body part. In this phase, the study will enhance balance strategy assessment in adults by integrating Motion Capture (MoCap) and AI clustering with the Clinical Test of Sensory Interaction on Balance (CTSIB). While traditional CTSIB is widely used, it relies on qualitative observations prone to observer bias. Our proposed framework introduces a data-driven approach involving: (1) Data Collection, (2) Feature Extraction [ankle, knee, and hip computed law of cosines], (3) Data Clustering, and (4) Evaluation. By extracting high-dimensional kinematic features at the ankle, knee, and hip using the Law of Cosines, this phase aims to establish an objective evaluation tool, this phase aims to establish an objective evaluation tool that reveals intricate balance patterns invisible to the naked eye, ultimately improving early fall risk detection.

The second phase applies the developed framework from the previous phase to explore more insight into the balance strategies in children aged 7-13 years-old, a critical period for postural development. Unlike adults, children's balance strategies are more nuanced and harder to classify through subjective observation. Using high-precision IMU sensors (Xsens, 17-sensor full-body configuration), we recorded 316,800 data points from 44 participants during the modified CTSIB (m-CTSIB). An unsupervised machine learning pipeline—incorporating advanced preprocessing and feature engineering on the new set of input features extracted from three rotational degrees of freedom (DoF), along with their joint descriptions with processing into three proposed temporal formats, and clustering algorithms (K-means, BIRCH, H-Clust)—was employed. This phase aims to identify "hidden" balance archetypes, providing deeper insights into how children adapt their joint kinematics under different sensory conditions.

3.2 Human Balance Strategies Through Clustering Technique

3.2.1 Build Up the Data Mining Framework Using Public Dataset

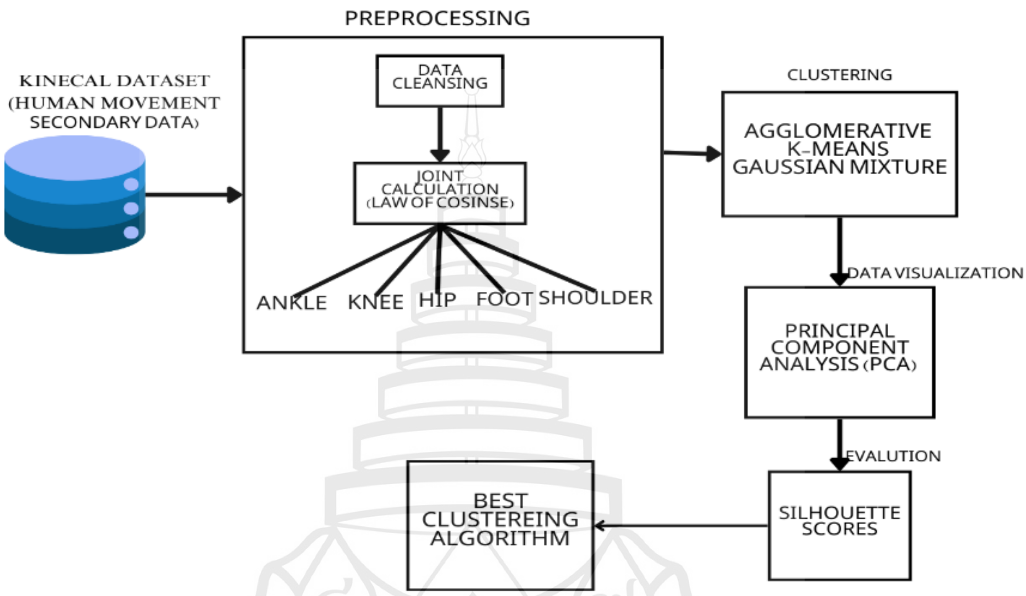

Figure 3.2 Proposed Research Framework Phase1

Phase1: The data used in this study were obtained from the KINECAL: Kinematic Measures for Assessing Balance Control dataset, available on PhysioNet (Version 1.0.3). This publicly accessible dataset contains detailed kinematic measures collected to evaluate balance control under various conditions. It provides a valuable resource for analyzing balance strategies and exploring patterns in postural stability.

Table 3.1 Example raw data phase 1

Joint	Tracked	X	Y	Z	px_X	px_Y
SpineBase	Tracked	0	0	0	1036.258	493.0001
SpineMid	Tracked	-0.00224	0.291509	-0.00078	1033.104	398.1467
Neck	Tracked	-0.00545	0.575756	-0.01303	1029.93	304.701
Head	Tracked	0.001759	0.700972	-0.02478	1031.485	262.6432
ShoulderLeft	Tracked	-0.16227	0.444199	-0.01383	979.79	348.9796
ElbowLeft	Tracked	-0.20362	0.213753	-0.00251	968.1944	425.052
WristLeft	Tracked	-0.2043	0.010479	-0.0573	969.8367	490.2945
HandLeft	Tracked	-0.20301	-0.04611	-0.06123	970.7574	508.9728
ShoulderRight	Tracked	0.147003	0.436634	-0.03363	1081.721	347.652
ElbowRight	Tracked	0.201387	0.206214	-0.01375	1100.705	423.7379
WristRight	Tracked	0.217076	-0.0236	-0.06395	1110.097	497.9714
HandRight	Tracked	0.197393	-0.05439	-0.06611	1103.917	508.3295
HipLeft	Tracked	-0.05187	-0.00176	-0.03285	1019.99	493.4725

Table 3.1 illustrates a representative sample of the extracted skeletal kinematics dataset used for joint angle calculation and movement feature engineering. For each tracked anatomical landmark, the dataset records the tracking status ('Tracked') to ensure data integrity and filter out occlusion artifacts.

The spatial positioning of each joint is captured across two distinct coordinate systems:

1. 3D Spatial Coordinates (X, Y, Z): Represent the relative positions of the joints in meters within the sensor's physical coordinate space.

2. 2D Pixel Coordinates (px_X, px_Y): Define the projected location of the joint centers on the 2D image plane in pixels, utilized for data verification.

The analysis begins with data preprocessing, which includes data cleansing to ensure the quality and consistency of the dataset. Joint angles at the ankle, knee, and hip are then calculated using the Law of Cosines, using five key reference points: the ankle, foot, knee, hip, and shoulder. These angles serve as the main features for identifying balance strategy use.

After preprocessing, three clustering algorithms are applied: Agglomerative Hierarchical, K-Means, and Gaussian Mixture Model. Principal Component Analysis (PCA) is then used to project the clustering results into two dimensions for visualization and interpretation. Finally, the performance of each algorithm is evaluated using the Silhouette Score to determine which algorithm best identifies distinct balance strategy patterns in the data.

The expected outcome of Phase 1 is not only the identification of three balance quality archetypes in adults, but more importantly, a validated methodological pipeline that confirms unsupervised clustering can objectively differentiate balance strategies from lower-limb kinematic data without relying on pre-assigned labels. Specifically, Phase 1 establishes three key decisions that directly inform Phase 2: the confirmation that k=3 or more clusters meaningfully represents distinct postural patterns, the identification of which clustering algorithm performs best on kinematic balance data, and the confirmation that joint angles at the hip, knee, and ankle — extracted as statistical features — are sufficient inputs for meaningful cluster separation. These validated decisions form the methodological foundation that Phase 2 builds upon. Rather than starting from scratch with the pediatric dataset, Phase 2 adopts the same core pipeline — kinematic feature extraction, unsupervised clustering, and internal validation metrics — and extends it with more advanced feature engineering and a broader set of algorithms to handle the greater complexity of children's balance data. In this way, Phase 1 acts as proof of concept, and Phase 2 acts as clinical application.

3.2.2 Identifying Children's Hidden Balance Strategies

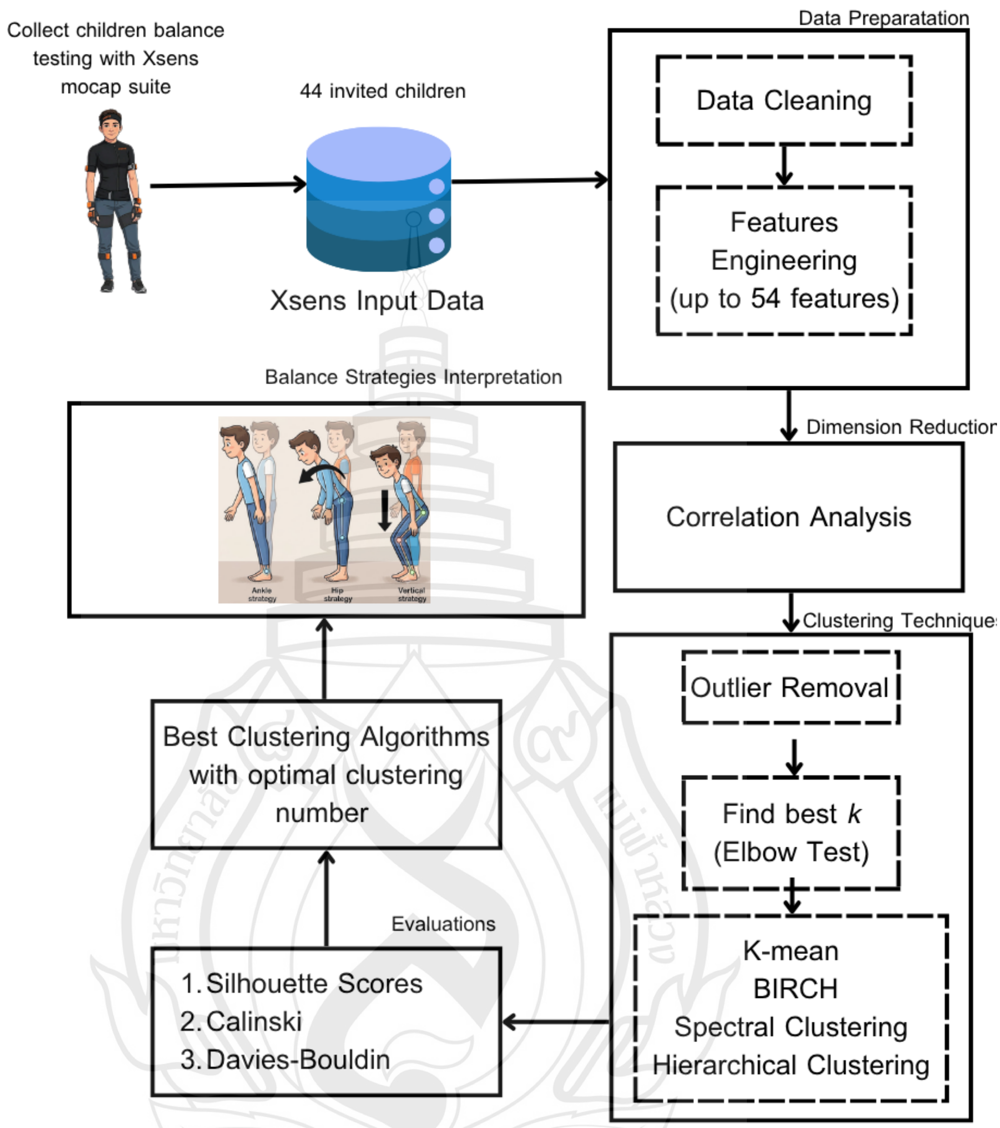

Figure 3.3 Proposed Research Framework Phase2

The proposed research begins with data collection and preprocessing, which includes data cleansing to ensure the reliability of the dataset. Feature engineering is then applied to extract kinematic profiles of the hip, knee, and ankle joints based on three rotational degrees of freedom, as described in Table 3.1. These three lower-limb joints were selected because they form a closed kinematic chain, meaning that movement or instability in one joint directly affects the others. Following feature engineering, dimensionality reduction is performed using Pearson correlation analysis to identify and remove redundant features, retaining only the parameters that contribute meaningful information to the clustering process.

The selection of hip, knee, and ankle joint angles as primary features is grounded in the classical postural control framework proposed by Horak and Nashner (1986), which characterizes reactive balance responses in terms of ankle, hip, and stepping strategies. As these balance strategies are kinematically expressed through coordinated movements at the lower-limb joints, joint-angle measurements at these three sites provide a direct and theoretically-grounded representation of the strategy employed by each participant in response to postural perturbation.

Table 3.2 Hip, Knee and Ankle joints kinetic features

Rotational Degrees of Freedom		**Joints Involves**
Parameters	***Description***	
Abduction/ Adduction (AA)	side-to-side movement relative to the body's midline	hip, knee, ankle
Internal/ External Rotation (IE)	twisting motion along the bone's long axis	hip, knee, ankle
Flexion/ Extension (FE)	forward and backward bending motion	hip, knee
Dorsiflexion/ Plantarflexion (DP)	involving pulling the toes upward or pointing them downward	ankle

In Phase 2, a secondary data of total 44 children (19 males and 25 females) elicited and studied in the "Application of Artificial Intelligence and Motion Analysis for Clinical Test of Sensory Interaction for Balance (CTSIB)" research with research ethics committee approval is adopted in this study. The demographic profile of the participants included an age range of 7–13 years-old, weights between 25–60 kg, and heights spanning 109–155 cm.

To capture their movement, we utilized 17 Xsense IMU sensors for a comprehensive full-body movement detection. The raw kinematic data was exported from Xsens MVN using the 'Joint ZXY' function to obtain precise joint angles in 3D space and data were sampled at 60 Hz to ensure high temporal resolution for motion analysis. This analysis focuses on lower-limb stability, selectively extracting data from the hip, knee, and ankle joints.

The participants were asked to perform four experimental conditions of the m-CTSIB explained in the previous section on a 30 second basis. During the data cleaning process, a standardized protocol was applied to participants who were unable to maintain their balance for the complete 30-second duration. In these instances, their kinematic values were set to zero for the remaining time of the trial to signify a loss of balance and ensure data consistency across the cohort.

This resulting in 176 comprehensive motion records. Each record yields 1,800 rows of kinematic data per trial.

Consequently, the dataset analyzed in this study comprises an extensive collection of 316,800 data frames, ensuring high temporal resolution for postural stability analysis.

Table 3.3 Example raw data phase2

Frame	Left Hip AA	Left Hip IE	Left Hip FE	Left Knee AA	Left Knee IE	Left Knee FE	Left Ankle AA	Left Ankle IE	Left Ankle DP
0	(-) 1.3387	18.062	5.6016	2.8569	0.3673	(-) 6.7811	2.6850	(-) 1.9618	(-) 0.5103
1	(-) 1.3622	18.013	5.5899	2.8582	0.3756	(-) 6.8239	2.6684	(-) 1.9749	(-) 0.5104
2	(-) 1.3325	17.980	5.6096	2.8539	0.3666	(-) 6.8472	2.6545	(-) 1.9874	(-) 0.5093
3	(-) 1.3111	17.949	5.6115	2.8512	0.3562	(-) 6.8545	2.6401	(-) 1.9999	(-) 0.5070
4	(-) 1.3113	17.923	5.6018	2.8455	0.3511	(-) 6.8539	2.6354	(-) 2.0029	(-) 0.5004
5	(-) 1.3197	17.885	5.5825	2.8444	0.3594	(-) 6.8525	2.6299	(-) 2.0019	(-) 0.4928
6	(-) 1.3143	17.833	5.5662	2.8465	0.3671	(-) 6.8532	2.6265	(-) 1.9982	(-) 0.4835
7	(-) 1.2956	17.792	5.5475	2.8531	0.3679	(-) 6.8574	2.6217	(-) 2.0048	(-) 0.4766

Table 3.3 shows the data in phase 2. After initial cropping 67, only 10 columns remain, focusing on the lower limbs (hip, knee, ankle). The choice of left, right, or right side is determined by expert analysis, which helps determine the child's primary problem or use, allowing for further analysis.

3.2.2.1 Test Procedure: m-CTSIB (Modified Clinical Test of Sensory Interaction and Balance) The Modified Clinical Test of Sensory Interaction in Balance (mCTSIB) is a clinical assessment to evaluate a human's postural stability by manipulating visual, somatosensory, and vestibular inputs. This assessment quantifies the efficacy of sensory integration across four distinct vestibular environmental conditions. Each participant performed the following four conditions:

1. Firm Surface, Eyes Open, Two Legs-standing (FiSEOTL): establishes a baseline static balance utilizing congruent somatosensory, visual, and vestibular information.

2. Firm Surface, Eyes Closed, Two Legs-standing (FiSECTL): eliminates visual orientation, forcing a reliance on somatosensory and vestibular feedback during static balance.

3. Foam Surface, Eyes Open, Two Legs-standing (FoSEOTL): destabilizes somatosensory input (proprioception), necessitating a primary reliance on visual and vestibular systems during static balance.

4. Foam Surface, Eyes Closed, Two Legs-standing (FoSECTL): attenuates both visual and somatosensory inputs during static balance, isolating the vestibular system as the primary source of balance control.

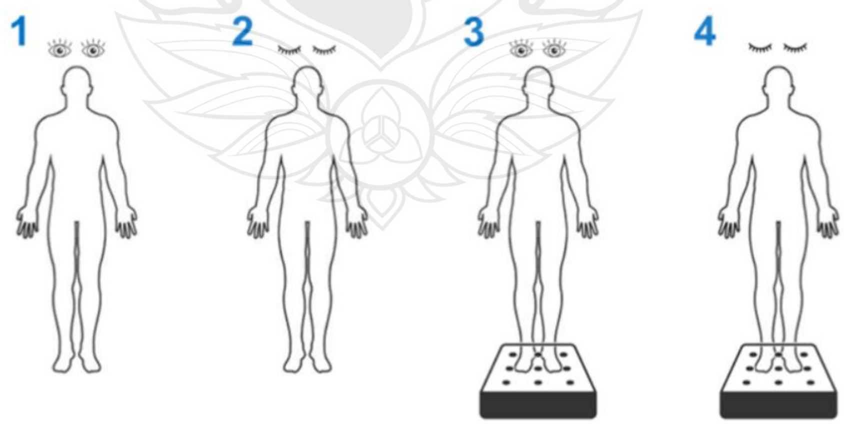

Source Souto (2024)

Figure 3.4 m-CTSIB Process

3.2.2.2 Setup Motion Capture: The full-body kinematic configuration utilized 17 wireless inertial measurement units (IMUs) secured to specific anatomical segments. Three sensors tracked the head, sternum, and pelvis, while six sensors mapped the upper extremities across the scapulae, upper arms, and forearms. For the lower extremities, six sensors were securely fixed to the thighs, shins, and feet to accurately record lower-limb joint kinematics. Lastly, two sensors were attached to the dorsal surface of the hands. All sensors were fastened using specialized elastic Velcro straps and a biomechanical body vest to minimize soft-tissue artifacts and sensor migration during balance testing.

Source Movella (n.d.)

Figure 3.5 Xsens MVN Awinda System Overview

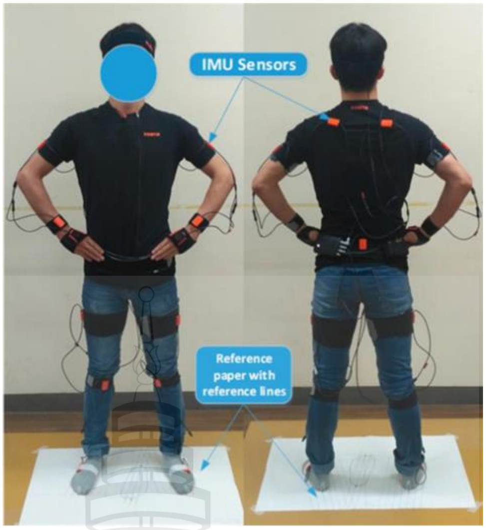

Source Xiong (2017)

Figure 3.6 Marker Placement in Xsens

The technical specifications regarding data formats, system recording protocols, and dataset management within this framework are operationalized as follows:

1. Data Output: CSV, BVH, XLSX or FBX.

2. Data Recording and Storage Motion capture recorded sessions in real-time, capturing detailed body movements during each m-CTSIB condition. Files were securely stored in digital format, labeled with unique participant IDs for anonymity.

3. Data Anonymization and Ethical Considerations All identifiable information was removed from the dataset before analysis to protect participant privacy

The processed data is then partitioned using four clustering algorithms; K-means, Spectral Clustering (SC), BIRCH, and Hierarchical Clustering (H-Clust). The optimal number of clusters (k) is determined using the Elbow Method, then, facilitate high-dimensional data interpretation, using Principal Component Analysis (PCA) for visualization. Finally, the clustering performance is quantitatively validated using the Silhouette Coefficient, Calinski-Harabasz Index, and Davies-Bouldin Score to determine the most effective algorithm for balance strategies characterization

The expected outcome of Phase 2 is the identification of distinct and previously hidden balance strategy archetypes in children aged 7 to 13 years-old that cannot be detected through standard clinical observation. Specifically, the framework is expected to reveal how children distribute postural control across the hip, knee, and ankle joints differently depending on the sensory condition, and to show that this distribution shifts in a consistent and meaningful way as sensory difficulty increases from firm-eyes-open to foam-eyes-closed. Beyond the archetype identification, the study expects to determine which combination of clustering algorithm, temporal feature format, and dimensionality reduction approach produces the most well-defined clusters for each m-CTSIB condition, providing a reproducible and objective protocol for pediatric balance strategy profiling. The outcome is a data-driven classification of children's postural behavior that gives clinicians a more precise and individualized picture of how each child manages balance under varying sensory demands — information that can serve as a foundation for more targeted and evidence-based rehabilitation planning in pediatric clinical care.

3.3 Data Mining Process

3.3.1 Data Cleansing

Phase 1: Data cleansing ensures the dataset is relevant and error-free for analysis. From table 3.1, the unused columns like Tracked, px_X, px_Y, and x were removed to simplify the data. Only essential joints—Ankle, Foot, Knee, Hip, and Shoulder are selected and processed in this study.

Phase2: To ensure the common features' scale, this research normalizes the joint angles using Min-Max scaling.

$$x_{norm} = \frac{x - x_{min}}{x_{min} - x_{max}}$$

1. $xnorm$ is the normalized value.
2. x is the original raw joint angle.
3. $xmax$ and $xmin$ are the maximum and minimum values of that feature across the entire dataset, respectively.

This step is crucial to ensure that joints with a larger range of motion (like the hip) do not numerically overwhelm joints with smaller, but equally significant, movements. Then, the outlier removal is implemented to eliminate signal noise or anomalous spikes caused by sensor drift. For these outliers, this research adjusted the values to a threshold of 0.05–0.1, depending on the specific distribution of each m-CTSIB condition. This process was done to ensure that the resulting groupings represent genuine pediatric balance patterns rather than measurement errors.

For the FiSEOTL condition, one subject's trial data was identified as having a failed set-zero calibration. As the affected temporal formats (D5I and S5A) could not be reliably corrected, the subject's data under this condition was excluded from those analyses, resulting in a reduced sample of 43 participants and 315,000 data frames for the D5I and S5A datasets. The OTM format, which aggregates data across the full trial duration and is less sensitive to calibration offset at a single time point, was retained with the full 44-participant dataset. Sensitivity checks confirmed that this exclusion did not materially alter the overall cluster structure in FiSEOTL.

3.3.2 Data Preprocessing

In Phase 1: the essential joints—Ankle, Foot, Knee, Hip, and Shoulder were computed based on the following calculations.

The lower-limb joints — ankle, knee, and hip — function as a hierarchical system for maintaining postural stability. The ankle serves as the primary stabilizer, continuously modulating muscle torque to keep the center of mass within the base of support during small, everyday postural perturbations. The knee acts as an intermediate link, redistributing forces between the ankle and hip and becoming increasingly engaged when balance demands exceed single-joint capacity, such as on unstable surfaces. The hip provides a secondary line of defense: when ankle-based corrections are insufficient — as occurs during eyes-closed or foam-surface conditions — the central nervous system shifts toward hip-level control, generating larger whole-body movements to recover equilibrium. In the context of CTSIB, where sensory availability is systematically reduced across conditions, the neuromuscular system becomes progressively more reliant on these joint-level adjustments, making lower-limb joint angles a direct kinematic indicator of the postural strategy employed under each sensory challenge.

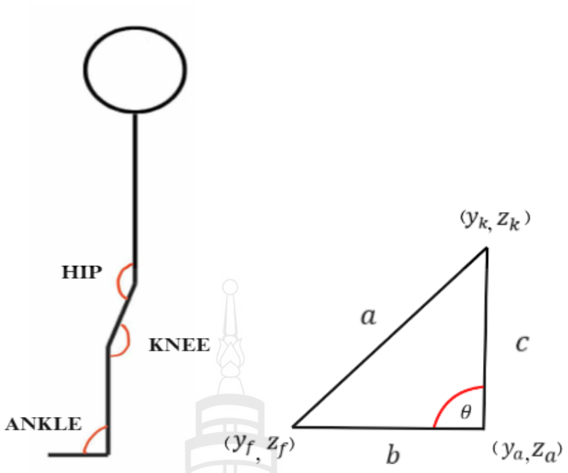

Figure 3.7 Joint angles and calculations

Data preprocessing involves structuring the dataset to ensure it is ready for analysis. Each joint is analyzed based on the angles formed by three key points. For the Ankle, the angles are determined using the positions of the Foot, Knee, and Ankle. Similarly, the Knee uses the points Knee, Ankle, and Hip, while the Hip is defined by the points Knee, Hip, and Shoulder. To compute these angles, the law of cosines is applied. For example, to find the Ankle angle, the distances between Foot to Knee, Knee to Ankle, and Ankle to Foot are calculated. These distances are then used to derive precise angles. This preprocessing step transforms the raw data into a meaningful structure, enabling accurate and interpretable analysis.

The distances become:

$$a = \sqrt{(y_k - y_a)^2 + (z_k - z_a)^2}$$

$$b = \sqrt{\left(y_a - y_f\right)^2 + \left(z_a - z_f\right)^2}$$

$$c = \sqrt{\left(y_f - y_k\right)^2 + \left(z_f - z_k\right)^2}$$

This equation applies to the law of cosines in a 2D plane to calculate the lengths of three sides of a triangle formed by three points in the coordinate system. Here's an explanation of each term: Suppose that

1. a is the length from knee to ankle y_k = y of knee, y_a = y of ankle and z_k = z of knee, z_a = z of ankle

2. b is the length from ankle to foot y_a = y of ankle, y_f = y of foot and z_f = z of foot, z_k = z of knee.

3. c is the length from hip to knee y_f = y of foot, y_k = y of knee and z_f = z of foot, z_k = z of knee

Angle calculation using the Law of Cosines:

$$\theta = arccos\left(\frac{(b^2 + c^2 - a^2)}{(2 \cdot b \cdot c)}\right)$$

1. cos(θ): The cosine of the angle θ opposite side a.
2. a: The side opposite the angle θ.
3. b and c: The other two sides of the triangle.

This equation relates the cosine of an angle in a triangle to the lengths of its sides.

Finding the Angle θ: To calculate the actual angle in radians (or degrees, depending on the context), take the arccosine (inverse cosine) of the value:

The function reverses the cosine operation, yielding the angle corresponding to the cosine value.

Table 3.4 Example of final input of phase 1

frame	ankle angles	knee angles	hip angles
1	133.327125	166.652512	161.093411
2	131.679999	166.800909	160.894593
3	130.894970	167.043557	160.735667
4	131.787875	167.067214	160.755493
5	134.622837	166.981551	160.827974
6	139.756106	167.153368	160.919845
7	107.222168	167.201215	160.941002
8	139.505765	167.065384	161.272785
9	107.146583	167.229073	161.286555
10	135.943748	167.547401	161.183646
11	132.621613	167.534818	161.262028
12	136.070361	167.535718	161.368598

Table 3.4 contains the final input data before clustering, after the processing steps have been completed. Each data point has approximately 600 frames, and the hip, knee, and ankle angles are calculated using the law of cosine.

In Phase 2: the three rotational degrees of freedom (DoF), along with their joint descriptions were computed into three proposed temporal formats based on the following calculations.

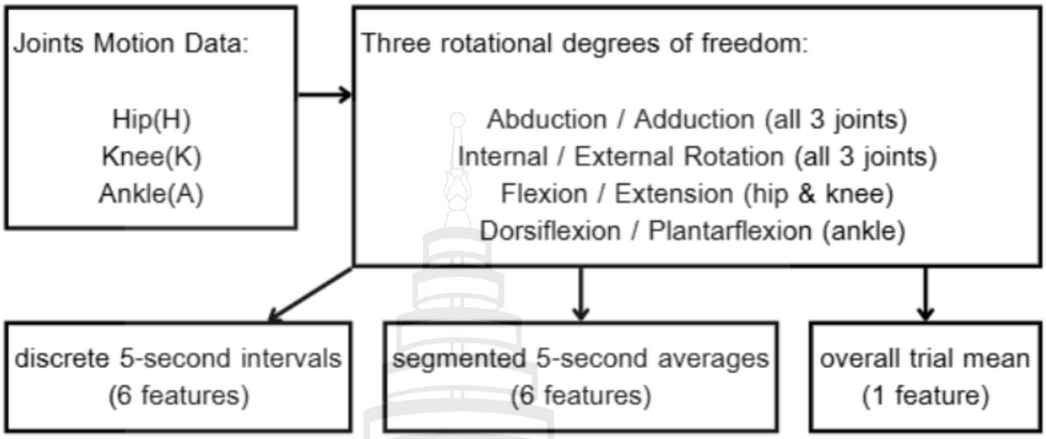

Figure 3.8 Features Engineering Framework

For each joint, as mentioned in Table 3.2, three rotational degrees of freedom (DoF) were extracted as input features based on their joint descriptions there are only 9 dimensions per condition for 44 participants. The construction of time-window-based features (5s, 10s, 15s, 20s, 25s, and 30s) for each joint-DoF combination resulted in a feature space of 54 dimensions per condition, derived from a sample of 44 participants. Each feature was further processed into three temporal formats;

1. Discrete 5-second intervals (D5I),

$$W_k = \{x_i | (k - 1 \cdot \Delta n < i \leq k \cdot \Delta n)$$

1) W_k is the sampling every fixed interval (5 seconds)
2) k is the interval index (1, 2, 3, …).
3) x_i represents the joint angle vector at time step (i = 5, 10, 15, …).
4) $\Delta n = 5 \times f$ is the total number of samples within a 5-second window of the equipment sampling rate f (650 Hz).

2. Segmented 5-second averages (S5A),

$$\bar{X}_{S5A,k} = \frac{1}{\Delta n} \sum_{i=(k-1)\Delta n+1}^{k\Delta n} xi$$

1) $\bar{X}_{S5A,k}$ is the mean vector of the joint angles in window k.
2) Δn is the number of data points in a 5 seconds-window *(5×f)*.
3) x_i is the joint angle at any time i.

3. Overall trial mean (OTM).

$$\bar{X}_{TM} = \frac{1}{N}\sum_{i=1}^{N} xi$$

1) $\bar{X}_{TM}$ is the cumulative average of joint angles throughout the entire test.
2) *N* is the total number of data points in one test

This feature engineering approach resulted in a total of 13 distinct features, allowing the clustering algorithms to analyze balance from different temporal perspectives; D5I capture sudden postural fluctuations, S5A identify momentary stability trends by filtering out signal noise, and the OTM characterizes the participant's global balancing performance.

4. Dimention Reduction

To ensure our clustering models weren't 'clouded' by redundant information, this study compared two different setups: one using the full suite of kinematic features and another refined through correlation analysis. In the second approach, we used Pearson correlation to spot variables that were too closely related, specifically those with a coefficient (r) higher than 0.90.

$$r = \frac{\sum(x_i - \bar{x})(y_i - \bar{y})}{\sqrt{\sum(x_i - \bar{x})^2 \sum(y_i - \bar{y})^2}}$$

1) r is the Pearson correlation coefficient.
2) xi, yi are the individual sample points of the two variables.
3) $\bar{x}$, $\bar{y}$ are the respective means of each variable.

Table 3.5 Example of final input of phase 2 (S5A)

Source Name	Hip Ab/Ad 10s	Hip In/Ex 10s	Hip Fle/Ext 10s	Knee Ab/Ad 10s	Knee In/Ex 10s	Knee Fle/Ext 10s	Ankle Ab/Ad 10s	Ankle In/Ex 10s	Ankle Dor/Pla 10s
1	-1.454	17.542	5.567	3.057	-0.005	-7.019	3.182	-2.162	-0.539
2	-4.698	-7.196	-6.125	1.152	-2.008	-8.217	9.214	-1.273	-2.160
3	-3.272	-29.643	-7.087	-7.466	1.203	0.402	4.097	19.681	3.243
4	1.036	-1.955	7.611	0.806	1.090	-5.243	1.672	3.298	2.794
5	-6.319	-5.524	3.186	-0.004	0.365	-3.121	2.868	-29.017	4.982
6	-2.783	-3.589	5.135	-1.250	1.617	-7.737	3.813	5.754	5.377

Table 3.5 is the final input before being used in S5A clustering, having already gone through the previous steps. The source name is the ID of the child participating in the test, and the actual data will have columns of 5s, 10s, 15s, 20s, 25s, and 30s, and approximately 44 rows in each dataset. The S5A and D5I datasets have similar formats, differing only in their calculation methods.

Table 3.6 Example of final input of phase 2 (OTM)

Source Name	Hip Ab/Ad	Hip In/Ex	Hip Fle/Ext	Knee Ab/Ad	Knee In/Ex	Knee Fle/Ext	Ankle Ab/Ad	Ankle In/Ex	Ankle Dor/Pla
1	6.466	24.036	10.601	3.647	-0.126	-6.906	8.486	-2.886	8.149
10	-4.644	10.457	8.158	2.348	1.192	9.447	12.800	-1.735	10.760
11	-2.130	5.766	7.943	-0.526	1.620	-4.036	11.045	-0.425	6.042
12	-2.184	8.187	8.961	0.714	1.470	-0.888	16.318	2.992	5.615
13	-1.397	5.331	5.538	0.134	0.243	-2.019	7.601	5.028	2.840

Table 3.6 is the final input before being used in OTM clustering, having already gone through the previous steps. The source name is the ID of the child who participated in the test, and the actual data will have approximately 44 rows.

3.3.3 Data Visualization using PCA

In this study, Principal Component Analysis (PCA) was employed to visualize the clustering results in a reduced-dimensional space. PCA transforms the original high-dimensional data into orthogonal components, allowing for a 2D representation while retaining the majority of the variance PCA-transformed data was visualized as a scatter plot, with each point representing an individual data sample and colored according to its cluster assignment. The clusters formed distinct groupings, indicating that the clustering algorithms effectively captured underlying patterns in the data

3.3.4 Clustering Techniques

To determine the most appropriate number of clusters (k), we employed the Elbow Method in which involved plotting the Distortion Score against a range of *k* values to identify the 'elbow' point, where increasing the number of clusters no longer yields a significant reduction in error.

In this study, we perform clustering using four distinct algorithms:

K-means:

$$\sum_{i=o}^{n} \min_{\mu_j \in C}(\|x_i^j - \mu_j\|^2)$$

1. C is the cluster.
2. n is the number of data points within that cluster.
3. xi,yi is the data point i in cluster j.
4. μj is the centroid of cluster j.

Spectral Clustering (S-Clust):

$$L = D - A$$

1. L is the Laplacian matrix
2. A is the adjacency matrix (or similarity matrix W), which indicates the proximity between points.
3. D is the degree matrix (the diagonal matrix that sums the rows in A).

BIRCH:

$$CF = (n, LS, SS)$$

1. CF is clustering feature
2. n is the number of data points in the sub-cluster.
3. $LS = \sum xi$ (Linear Sum of data points)
4. $SS = \sum xi$ (Square Sum of data points)

Hierarchical Clustering (H-Clust):

$$d(u,v) = \sqrt{\frac{|u||v|}{|u| + |v|}||x_u - x_v||}$$

1. $d(u,v)$ is the distance between group u and v
2. u and v are the two groups being merged.
3. $|u|$ and $|v|$ are the number of members in each group.
4. xu, xv is the centroid of each group.

Gaussian Mixture Model (GMM)

$$p(x) = \sum_{K=1}^{K} \pi_k N(x|\mu_k \sum k)$$

1. $\boldsymbol{p}(\boldsymbol{x})$The probability density function of the data point x

2. $\sum_{K=1}^{K}$:The summation symbol (Sigma), representing the total sum computed across all clusters from cluster 1 to *K*.

3. $\boldsymbol{\pi_k}$: The mixing coefficient (or mixing weight) of the k cluster, which represents the prior probability of a data point belonging to that specific cluster.

4. $\boldsymbol{N}(\boldsymbol{x}|\boldsymbol{\mu_k} \sum \boldsymbol{k})$: The Gaussian (Normal) distribution function of the $\sum \boldsymbol{k} - \boldsymbol{\mu_k}$ cluster, where:

1) $\boldsymbol{\mu_k}$mean or midpoint of the cluster

2) $\sum \boldsymbol{k}$ variance matrix, which indicates the "shape" and "direction" of the cluster

3.4 Evaluation and Visualization

To assess the quality of the clusters on different planar of kinematics and determine the optimal algorithm, we utilize three internal validation metrics focusing on how well-separated and cohesive the identified balance groups are.

Silhouette Coefficient (SC) measures how similar an individual child's balance movement profile is to their own cluster compared to other clusters. A score closer to +1 indicates a perfect assignment.

$$SC = \frac{b(i) - a(i)}{\max(a, b)}$$

Calinski-Harabasz Index (CH), also known as the Variance Ratio Criterion, will be used to calculate the ratio of the sum of between-clusters dispersion and of within-cluster dispersion. Higher scores indicate that clusters are dense and well-separated.

$$CH = \frac{SS_B}{SS_W} \times \frac{N - k}{k - 1}$$

Davies-Bouldin Score (DB) will signify the average 'similarity' between clusters. Unlike the others, a lower DB score is better, as it means the clusters are distinct and do not overlap.

$$DB = \frac{1}{k}\sum_{i=1}^{k} max_{i\neq j}\left(\frac{S_i + S_j}{d_{ij}}\right)$$

Finally, the Principal Component Analysis (PCA) is applied to project the high-dimensional kinematic data into a 2D visual space in which qualitative validation can visually inspect the distance between different strategies.

3.5 Research Outcome

The overall expected outcome of this thesis is a validated, objective framework for identifying human balance strategies from motion capture data across both adult and pediatric populations.

From Phase 1, the expected outcome is confirmed proof of concept that unsupervised clustering can objectively separate adults into distinct balance quality groups — Good Balance, Slight Unbalance, and Poor Balance — based on lower-limb joint angle data alone, without requiring pre-assigned clinical labels. This phase is expected to establish the core pipeline as a reliable foundation for Phase 2.

From Phase 2, the expected outcome is the identification of hidden balance strategy archetypes in children across four m-CTSIB sensory conditions. The framework is expected to reveal how children's postural strategies shift consistently as sensory difficulty increases, and to determine the most effective algorithm and feature combination for each condition.

At the thesis level, both phases together are expected to demonstrate that unsupervised machine learning applied to motion capture data can provide objective and clinically meaningful insights into balance strategy use that traditional observation-based assessment cannot offer, and to provide a foundation for future development of a supervised classification tool for use in clinical rehabilitation planning.

CHAPTER 4

EXPERIMENTAL RESULTS

This research framework is divided into two interconnected phases, moving from macro-level population grouping to micro-level joint coordination analysis under sensory deprivation. In the first phase, unsupervised machine learning models (such as K-Means, Agglomerative Clustering, and GMM) are applied to evaluate baseline joint kinematics. Through statistical metrics like the Silhouette Score and the Elbow Method, the subject population is optimally categorized into three main balance quality groups: Good Balance (stable control), Slightly Unbalanced (moderate variability), and Poor Balance (high dispersion with frequent corrections).

Building directly upon these baseline groups, the second phase serves as the explanatory module to examine how individual joints adapt when primary senses are systematically challenged. Utilizing the modified Clinical Test of Sensory Interaction and Balance (m-CTSIB) protocol combined with a 17-sensor Xsens full-body motion capture system, this phase tracks multi-planar angular variations across the hip, knee, and ankle. The results deconstruct how motor strategies shift across four difficulty thresholds—ranging from a core-controlled Mixed Strategy (Hip-Ankle) under normal conditions, to a localized Ankle Strategy as sensory inputs are progressively compromised.

The connection between the two phases provides a comprehensive diagnostic pipeline where Phase 1 defines "who" is unstable, and Phase 2 explains "why" by isolating the exact biomechanical root causes. Under the most strenuous condition of combined visual and somatosensory deprivation (FoSECTL), Phase 2 successfully isolates critical compensatory profiles—such as highly unstable individuals who violently bend their knees as an emergency recovery mechanism. This offers a direct, joint-level explanation for the global "Poor Balance" traits identified in Phase 1, bridging the gap between automated data clustering and targeted clinical fall-risk evaluation.

4.1 Build Up the Data Mining Framework Using Public Dataset

Phase 1: Clustering Result and Evaluation

Table 4.1 Mean Silhouette Scores of Clustering Algorithms with Varying Values

Algorithm	k=2	k=3	k=4	k=5	k=6
Agglomerative Clustering	0.57674	0.42413	0.37135	0.3409	0.32408
Gaussian Mixture	0.48643	0.35626	0.3001	0.27619	0.25693
K-Means	0.54483	0.44295	0.38181	0.36847	0.35297

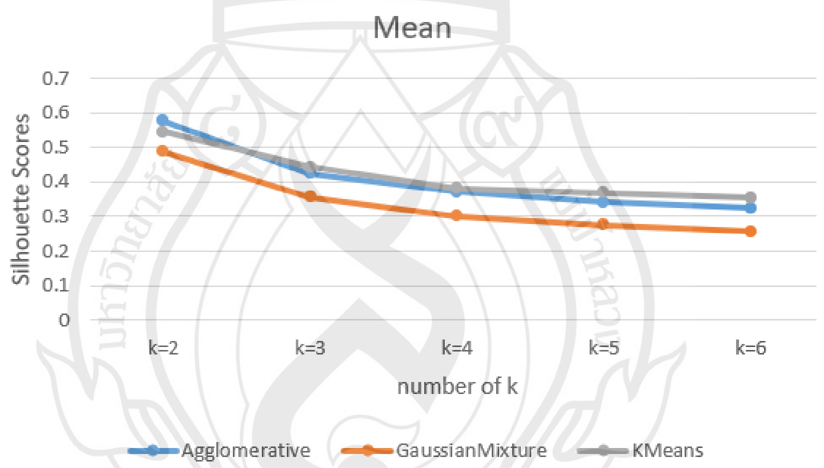

Figure 4.1 Elbow Test of Mean Silhouette Scores

Although the Silhouette Scores show higher values at k=2 across all algorithms, this alone is not sufficient to determine the optimal number of clusters. The Elbow Method is also required to identify the point where adding more clusters no longer significantly improves compactness. As shown in Figure 4.1, the elbow test indicates that k=3 is the most appropriate number of clusters for this study. This result is consistent with the gradual decline observed in the Silhouette Scores, confirming that k=3 provides the best balance between cluster compactness and separation.

By combining the quantitative Silhouette Scores with the elbow test results, k=3 is identified as the optimal number of clusters for the clustering analysis in this research.

Next, we obtained the Distraction Analysis, which revealed 3 distinct groups. There are 3 groups in total:

Group 1: This group has a fairly good balance

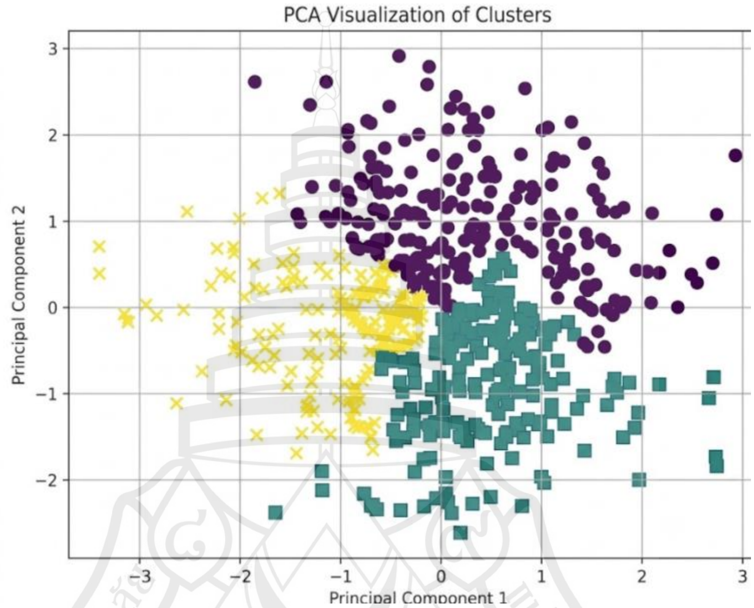

Figure 4.2 Example of Clustering result of Group 1

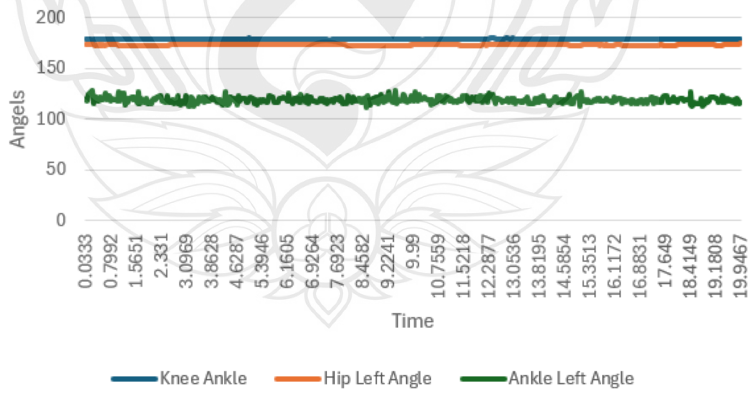

Figure 4.3 Example of knee, hip, and ankle angles of raw data Group 1

From Figure 4.2, Group 1 in the PCA plot shows minimal data dispersion, with data points clustering tightly in a specific region. This indicates that individuals in this group have consistent balance strategies with little variation in postural adjustments.

The tight grouping suggests that they rely on a single, well-executed balance strategy, and their balance control is efficient and stable under the tested conditions. This places Group 1 in the Good Balance category.

From Figure 4.3, when compared with the raw data, the balance signal is highly stable with good postural control. The balance strategy used is consistent and requires minimal corrective adjustments. This confirms that individuals in this group belong to the Good Balance category.

Group 2: This group has a slightly unbalanced balance.

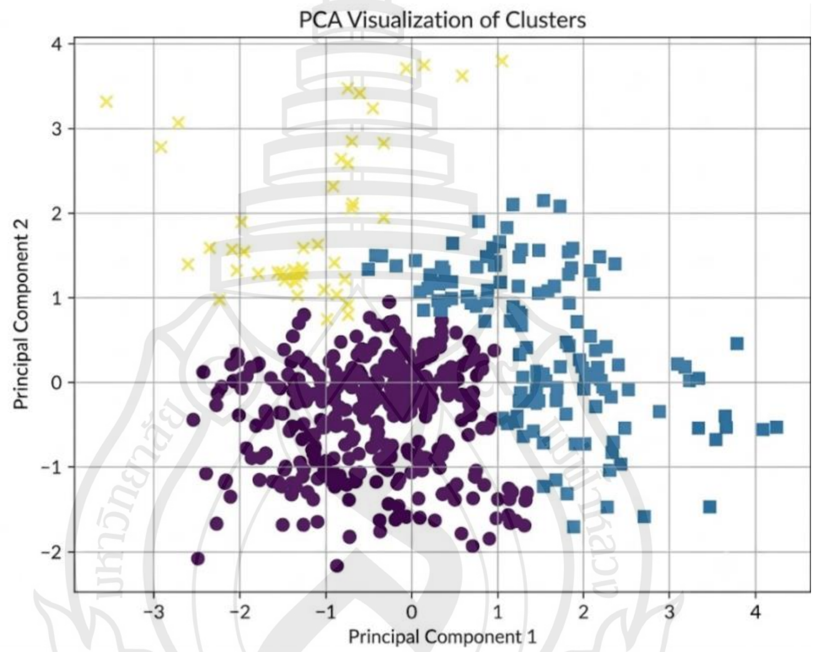

Figure 4.4 Example of Clustering result of Group 2

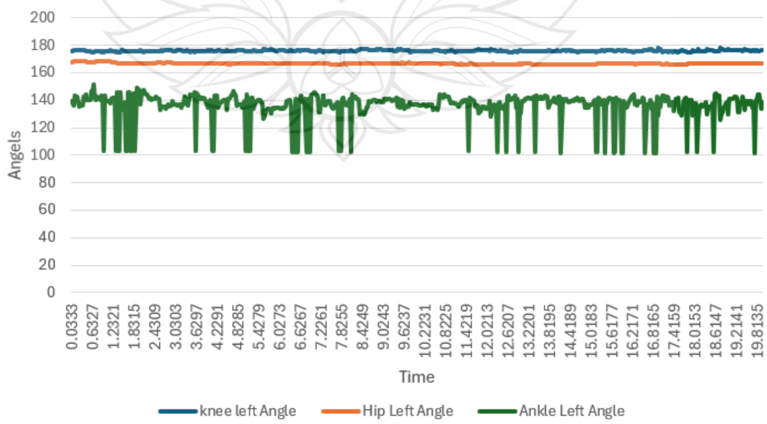

Figure 4.5 Example of knee, hip, and ankle angles of raw data Group 2

From Figure 4.4, the data shows greater dispersion than Group 1 in the PCA plot. The reduced density compared to Group 1 suggests increased variability in the balance strategies employed by individuals in this group. This dispersion indicates that while balance is still maintained, there is a notable reliance on a strategy. These individuals may exhibit stable control in most conditions but require specific adjustments to maintain balance effectively.

From Figure 4.5, analysis of the raw data reveals that balance strategies are beginning to play a noticeable role in maintaining stability. Although overall balance remains relatively stable, the use of a single prominent strategy can be observed. This suggests that this individual falls into the Slightly Unbalanced Group.

Group 3: This group uses a mix of strategies Poor Balance Group.

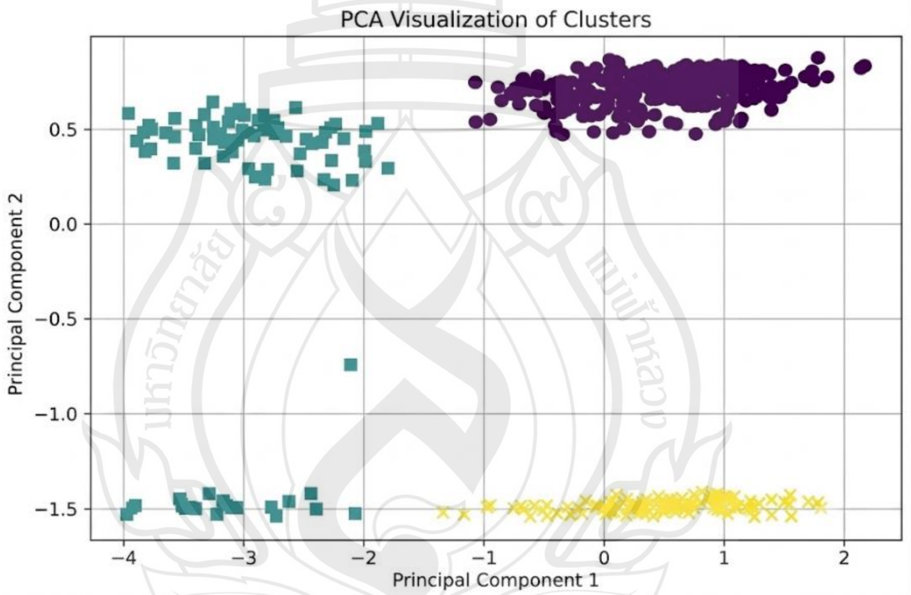

Figure 4.6 Example of Clustering result of Group 2

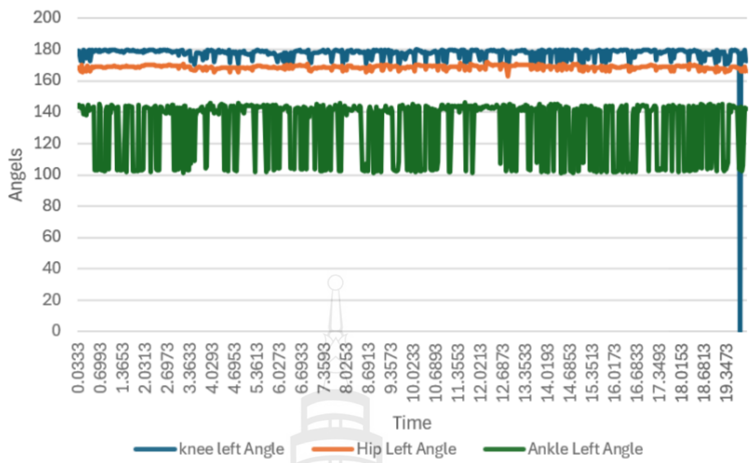

Figure 4.7 Example of knee, hip, and ankle angles of raw data Group 3

From Figure. 4.6, the PCA plot displays higher data dispersion than both Groups 1 and 2. This increased variability suggests a more complex and dynamic use of balance strategies, with individuals employing multiple approaches to maintain stability. Despite the broader distribution, there is still a degree of density and a tendency for data points to cluster in a specific region. This indicates that while variability exists, certain patterns or combinations of strategies. These characteristics are indicative of individuals in the "poor balance" category, where frequent and varied adjustments are necessary to compensate for instability.

From Figure. 4.7, examination of the raw data highlights the frequent and diverse use of multiple balance strategies to maintain stability. The angles and movements indicate a mix of strategies being employed to compensate for instability. This suggests that this individual belongs to the Poor Balance Group, where balance is less stable, and strategies are used more frequently to manage postural stability.

4.2 Identifying Children's Hidden Balance Strategies

This part collected the children's static balance movement using the Xsens motion capture and extracted it into three types of DoF in which, later, preprocessed into three temporal formats and modified based on its correlation. In total, there are 54 distinct features used as the input. The participants were asked to perform their static balance based on four m-CTSIB environmental conditions to find the best algorithms suitable for each balance strategies partitioning.

4.2.1 FiSEOTL Condition

Table 4.2 Two Legs with Eyes Open on a Hard Surface

Temporal Formats	**No. of parameters**	**Best Algorithm**	**Outlier Threshold**	**Best *k***	**Evaluation Score**		
					SC	***CH***	***DB***
non-correlated D5I	54	Spectral	0.1	3	0.34	15.61	0.67
correlated D5I	14	H-Clust	0.1	4	0.37	26.30	0.89
non-correlated S5A	54	K-means	0.1	4	0.32	22.80	0.86
correlated S5A	13	BIRCH/ Spectral	0.05	4	**0.42**	**29.68**	**0.58**
OTM	9	BIRCH	0.05	4	0.38	26.60	0.64

Table 4.2 shows the clustering results of the two legs standing with eyes open on the hard surface. Full results can be seen on appendix A Table A1. There were five district temporal formats with and without the correlation execution. The non-correlated S5A yielded the best result on Silhouette Coefficient as 0.420, Calinski-Harabasz as 29.677 and Davies-Bouldin score as 0.578.the best result in correlated S5A type where parameters were reduced using correlation.

Table 4.3 Median Joint of Tri-planar Kinematics by Cluster of FISEOTL

Cluster	Frontal plane			Transverse plane			Sagittal plane		
	Hip Ab/Ad	**Knee Ab/Ad**	**Ankle Ab/Ad**	**Hip IR/ER**	**Knee IR/ER**	**Ankle IR/ER**	**Hip F/E**	**Knee F/E**	**Ankle DF/PF**
CA0	(-) 2.78	0.35	3.33	2.50	1.52	(-) 0.43	1.90	(-) 6.93	0.97
CA1	(-) 2.94	0.67	4.45	(-) 2.94	4.34	4.51	(-) 2.94	4.41	4.60
CA2	(-) 1.40	0.82	3.522	(-) 1.40	3.13	3.88	(-) 1.40	3.27	4.09
CA3	0.63	(-) 5.21	(-) 11.22	0.57	(-) 10.87	(-) 11.22	0.43	(-) 11.05	(-) 11.22

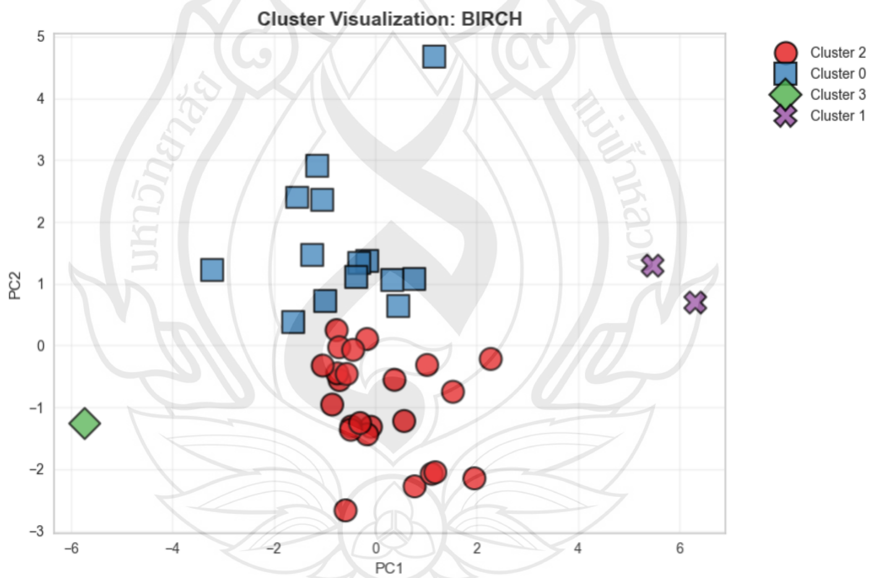

Figure 4.8 Four Clusters of FiSEOTL testing from the BIRCH algorithm with k=4

Analysis of Table 4.3 revealed different joint stabilization patterns among the four clusters on different planar of kinematics using mathematical metrics and analysis. CA0 used a Mixed Strategy, combining hip rotation (Hip Ab/Ad = −2.78°, Hip IR/ER = 2.50°, Hip F/E = 1.90°) with a relatively large knee flexion contribution (Knee F/E =

−6.93°), while ankle involvement remained low (Ankle IR/ER = −0.43°, Ankle DF/PF = 0.97°).

Clusters CA1 and CA2 both relied on a coordinated hip-pivot pattern, where Hip Ab/Ad, IR/ER, and F/E values were nearly identical within each cluster (CA1 = −2.94° across all three planes; CA2 = −1.40°/1.40°/1.40°), accompanied by moderate, comparable knee and ankle excursions (CA1: 0.67°–4.60°; CA2: 0.82°–4.09°). CA1 showed slightly larger values across nearly all parameters than CA2, suggesting a more pronounced version of the same hip-led strategy.

Cluster CA3 showed the most distinct pattern: Hip Ab/Ad, IR/ER, and F/E values were the smallest in the dataset (0.43°–0.63°), indicating a stabilized, near-fixed hip-trunk segment. In contrast, knee and ankle values were the largest across the entire table — Knee IR/ER (−10.87°), Knee F/E (−11.05°), and Ankle Ab/Ad/IR/ER/DF/PF (−11.22° each) — roughly 2 to 17 times higher than the corresponding values in CA0–CA2. Rather than achieving stability through generalized rigidity, CA3 appears to fix the hip/trunk while relying on substantially larger compensatory movements at the knee and ankle to recover balance.

Analysis of Table 4.3 identified three balance patterns using a tri-planar kinematic analysis across the frontal, transverse, and sagittal planes.

In the frontal plane, Hip Ab/Ad values for CA0 (−2.78°), CA1 (−2.94°), and CA2 (−1.40°) are small and negative, indicating mild, comparable hip adduction across these clusters. CA3, by contrast, is the only cluster with a positive Hip Ab/Ad (0.63°), while its Knee Ab/Ad (−5.21°) and Ankle Ab/Ad (−11.22°) are substantially larger in magnitude and in the opposite direction compared to CA0–CA2 (range: 0.35°–0.82° and 3.33°–4.45°, respectively).

In the transverse plane, Hip IR/ER differentiates the clusters: CA0 shows internal rotation (2.50°), CA1 and CA2 show external rotation (−2.94° and −1.40°), while CA3 remains near neutral (0.57°). Knee IR/ER is moderate and positive across CA0–CA2 (1.52°–4.34°), whereas CA3 reaches a markedly larger negative value (−10.87°). Ankle IR/ER follows a similar pattern: low in CA0 (−0.43°), moderate in CA1 (4.51°) and CA2 (3.88°), and largest in CA3 (−11.22°).

In the sagittal plane, CA0 shows the largest negative Knee F/E among CA0–CA2 (−6.93°) with near-zero ankle involvement (0.97°), indicating a knee-dominant sagittal response with minimal ankle contribution. CA1 and CA2 show moderate, positive values across both knee (4.41° and 3.27°) and ankle (4.60° and 4.09°), suggesting balanced sagittal engagement. CA3 presents the most extreme values: Knee F/E (−11.05°) and Ankle DF/PF (−11.22°) are the largest in the dataset, while Hip F/E (0.43°) remains the smallest across all clusters.

4.2.2 FiSECTL condition

Table 4.4 Two Legs With Eyes Closed On a Hard Surface

Temporal Formats	**No. of parameters**	**Best Algorithm**	**Outlier Threshold**	**Best *k***	**Evaluation Score**		
					SC	***CH***	***DB***
non-correlated D5I	54	Spectral	0.08	4	0.383	20.355	0.983
correlated D5I	12	Spectral	0.05	3	**0.548**	22.759	**0.448**
non-correlated S5A	54	BIRCH /H-Clust	0.05	4	0.383	26.770	0.686
correlated S5A	10	BIRCH /H-Clust	0.05	4	0.400	**31.962**	0.786
OTM	9	Spectral	0.05	3	0.446	21.913	0.613

Table 4.4 shows the experimental results for two-legs with eyes closed on a firm surface. Full results can be seen in appendix A Table A2. Five temporal formats were tested, both with and without correlation filtering: non-correlated D5I, correlated D5I, non-correlated S5A, correlated S5A, and TM. The best result was found in the correlated D5I format with 12 parameters, using the Spectral algorithm at k=3, which achieved a Silhouette Coefficient of 0.548, a Calinski-Harabasz Index of 22.759, and a Davies-Bouldin Score of 0.448.

Table 4.5 Median Joint of Tri-planar Kinematics by Cluster of FISECTL

Cluster	Frontal plane			Transverse plane			Sagittal plane		
	Hip Ab/Ad	**Knee Ab/Ad**	**Ankle Ab/Ad**	**Hip IR/ER**	**Knee IR/ER**	**Ankle IR/ER**	**Hip F/E**	**Knee F/E**	**Ankle DF/PF**
CB0	(-) 3.02	0.771	4.339	4.61	(-) 0.685	(-) 2.810	(-) 3.251	(-) 13.225	(-) 0.410
CB1	(-) 2.13	(-) 0.404	1.448	(-) 2.134	1.340	1.536	(-) 2.097	1.448	1.598
CB2	(-) 2.08	0.642	3.468	(-) 2.083	3.384	3.546	(-) 2.065	3.468	3.603

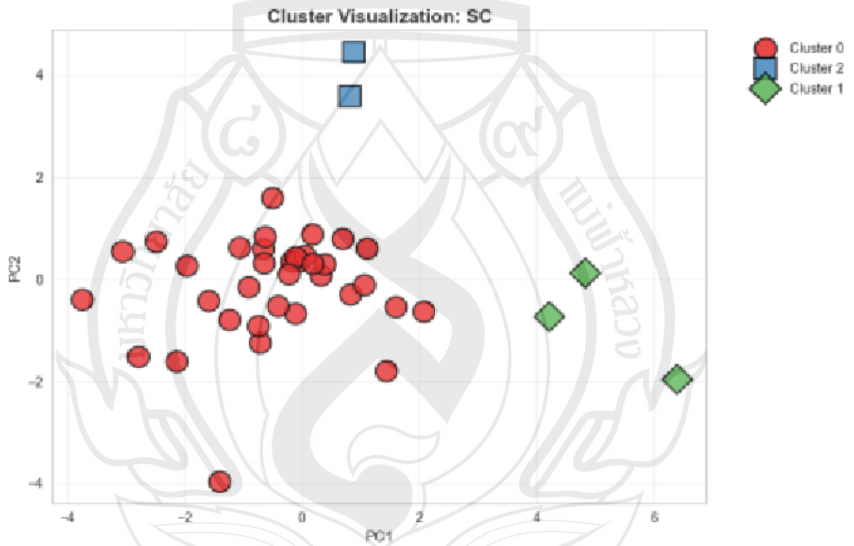

Figure 4.9 Three Clusters of FiSECTL testing from the Spectral algorithm with k=3

Analysis of Table 4.5 identified three balance patterns on different planar of kinematics using mathematical metrics and analysis. Cluster CB0 represented a Mixed Strategy, characterized by an extreme Knee F/E value (−13.225°) — the largest in the entire table, several times greater than any other parameter — combined with moderate hip rotation (Hip Ab/Ad = −3.02°, Hip IR/ER = 4.61°, Hip F/E = −3.251°) and notable ankle abduction/adduction (Ankle Ab/Ad = 4.339°), while Ankle IR/ER and Ankle DF/PF remained minimal (−2.810° and −0.410°).

Clusters CB1 and CB2 both relied on a similar coordinated hip-pivot pattern, with nearly identical hip values across all three planes (CB1 ≈ −2.10° to −2.13°; CB2 ≈ −2.07° to −2.08°). The two clusters are differentiated by the magnitude of knee and ankle involvement: CB1 shows smaller knee and ankle excursions (1.340°–1.598°), reflecting a subtle, low-amplitude Ankle-Knee Strategy, while CB2 shows roughly double these values (3.384°–3.603°), indicating a more pronounced version of the same Ankle-Knee Strategy with greater distal joint involvement.

Analysis of Table 4.5 identified three balance patterns using a tri-planar kinematic analysis across the frontal, transverse, and sagittal planes.

In the frontal plane, Hip Ab/Ad values are small and negative across all three clusters (CB0 = −3.02°, CB1 = −2.13°, CB2 = −2.08°), indicating comparable mild hip adduction throughout. Knee Ab/Ad remains small across all clusters (−0.404° to 0.771°). The primary differentiation in this plane comes from Ankle Ab/Ad: CB0 shows the largest value (4.339°), CB2 an intermediate value (3.468°), and CB1 the smallest (1.448°).

In the transverse plane, Hip IR/ER most clearly separates CB0 from CB1 and CB2: CB0 shows internal rotation (4.61°), whereas CB1 (−2.134°) and CB2 (−2.083°) both show external rotation of near-identical magnitude. Knee IR/ER and Ankle IR/ER follow a consistent ascending gradient from CB0 to CB2 — CB0 presents negative values (−0.685° and −2.810°), CB1 shows moderate positive values (1.340° and 1.536°), and CB2 shows the largest positive values (3.384° and 3.546°).

In the sagittal plane, the most clinically striking finding is Knee F/E in CB0 (−13.225°) — the largest value in the entire table, approximately 3.8 times greater in magnitude than CB2 (3.468°) and in the opposite direction. Despite this, CB0's Ankle DF/PF remains near zero (−0.410°), indicating that the sagittal response in CB0 is concentrated at the knee rather than distributed across the lower limb. CB1 and CB2 show moderate, positive values for both Knee F/E (1.448° and 3.468°) and Ankle DF/PF (1.598° and 3.603°), with CB2 approximately double CB1 across both parameters. Hip F/E is consistently small and negative across all clusters (−2.065° to −3.251°), indicating minimal hip sagittal contribution regardless of cluster.

4.2.3 FoSEOTL condition

Table 4.6 Two Legs with Eyes Open on a Foam Surface

Temporal Formats	No. of parameters	Best Algorithm	Outlier Threshold	Best *k*	Evaluation Score		
					SC	***CH***	***DB***
non-correlated D5I	54	H-Clust	0.05	4	0.335	25.841	0.956
correlated D5I	20	H-Clust	0.05	4	0.404	**28.940**	**0.663**
non-correlated S5A	54	K-mean	0.05	4	0.334	26.989	0.924
correlated S5A	9	BIRCH	0.05	4	**0.429**	21.151	0.720
OTM	9	Spectral	0.05	4	0.409	21.037	0.734

Table 4.6 shows the experimental results for two-leg standing with eyes open on a foam surface. Full results can be seen on appendix A Table A3. Five temporal formats were tested, both with and without correlation filtering: non-correlated D5I, correlated D5I, non-correlated S5A, correlated S5A, and TM. The best result was found in the correlated D5I format, which achieved a Silhouette Coefficient of 0.429, a Calinski-Harabasz Index of 28.940, and a Davies-Bouldin Score of 0.663. Analysis of Table 4.7 identified three distinct postural control patterns. Cluster 0 used a Mixed Strategy, integrating hip and ankle movement under stiff knee conditions for maximum stability. Cluster 1 used an energy-efficient Ankle Strategy with minimal movement for normal support. Cluster 2 used the more flexible Ankle-Knee Strategy to manage continuous momentum.

Table 4.7 Median Joint of Tri-planar Kinematics by Cluster of FOSEOTL

	Frontal plane			Transverse plane			Sagittal plane		
Cluster	**Hip Ab/Ad**	**Knee Ab/Ad**	**Ankle Ab/Ad**	**Hip IR/ER**	**Knee IR/ER**	**Ankle IR/ER**	**Hip F/E**	**Knee F/E**	**Ankle DF/PF**
CC0	(-) 4.617	0.043	4.838	4.355	0.905	6.671	13.456	8.734	10.965
CC1	(-) 2.978	1.466	6.680	(-) 1.384	3.195	6.728	(-) 0.148	5.020	6.943
CC2	(-) 1.223	2.592	6.426	0.014	3.975	5.923	1.295	5.344	5.414
CC3	(-) 3.580	(-) 6.231	(-) 8.000	(-) 4.562	(-) 6.956	(-) 6.039	(-) 5.330	(-) 7.762	(-) 4.179

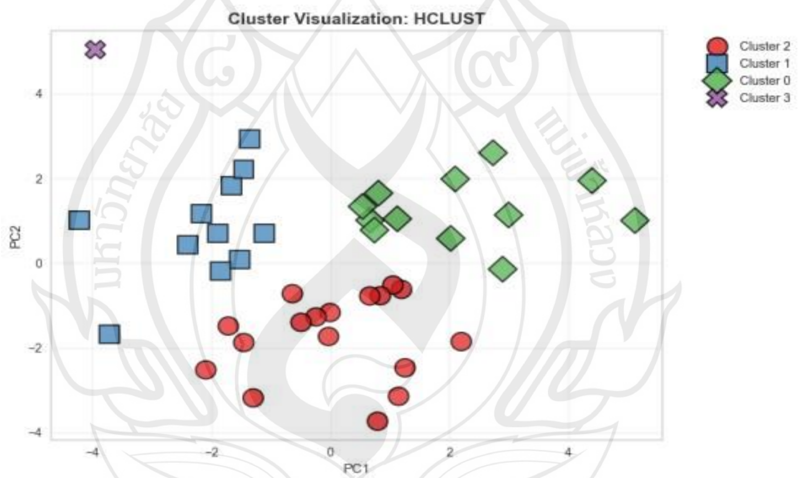

Figure 4.10 Four Clusters of H-Clust testing from the K-mean algorithm with k=4

The analysis reveals four distinct postural control identities on different planar of kinematics using mathematical metrics and analysis. Cluster CC0 represents the Highest Balance Strategy, dominated by Hip F/E (13.456°) and Ankle DF/PF (10.965°) the two largest values in the entire table — together with the highest Knee F/E value (8.734°) of any cluster. While Knee Ab/Ad (0.043°) and Knee IR/ER (0.905°) remain minimal, the substantial Knee F/E value indicates the knee is not uniformly "stiff" but contributes significantly in the sagittal plane, consistent with a Mixed, multi-joint strategy integrating hip, knee, and ankle torque for maximum-amplitude balance recovery.

Clusters CC1 and CC2 both rely on lower-leg strategies with minimal hip involvement but differ in their relative ankle and knee contributions. CC1 shows the largest ankle values among the two (Ankle Ab/Ad = 6.680°, Ankle IR/ER = 6.728°, Ankle DF/PF = 6.943°) alongside comparatively lower knee values (Knee Ab/Ad = 1.466°, Knee IR/ER = 3.195°, Knee F/E = 5.020°), indicating an Ankle-dominant strategy. CC2 shows higher knee involvement (Knee Ab/Ad = 2.592°, Knee IR/ER = 3.975°, Knee F/E = 5.344°) alongside slightly lower ankle values (Ankle Ab/Ad = 6.426°, Ankle IR/ER = 5.923°, Ankle DF/PF = 5.414°), reflecting a more balanced Ankle-Knee Strategy.

Cluster CC3 stands apart as the only cluster in which every parameter is negative, indicating a movement direction opposite to CC0–CC2 across all hip, knee, and ankle planes. Several values are also among the largest magnitudes in the table (Ankle Ab/Ad = −8.000°, Knee F/E = −7.762°, Knee IR/ER = −6.956°), suggesting a distinct, oppositely oriented compensatory pattern rather than simple joint-locking.

Analysis of Table 4.7 reveals four distinct postural control patterns using a tri-planar kinematic analysis across the frontal, transverse, and sagittal planes.

In the frontal plane, Hip Ab/Ad is negative across all clusters, with CC0 showing the largest adduction (−4.617°) and CC2 the smallest (−1.223°). Knee Ab/Ad is near zero in CC0 (0.043°) and increases progressively through CC1 (1.466°) and CC2 (2.592°). CC3, however, presents negative values in both Knee Ab/Ad (−6.231°) and Ankle Ab/Ad (−8.000°) — the largest magnitudes in the frontal plane and in the opposite direction from CC0–CC2 (range: 4.838°–6.680°).

In the transverse plane, Hip IR/ER differentiates the clusters clearly: CC0 shows the largest internal rotation (4.355°), CC2 remains near neutral (0.014°), CC1 shows mild external rotation (−1.384°), and CC3 shows the largest external rotation (−4.562°). Knee IR/ER is near zero in CC0 (0.905°) and increases through CC1 (3.195°) and CC2 (3.975°), while CC3 again presents a large negative value (−6.956°). Ankle IR/ER is similarly large and positive in CC0 (6.671°) and CC1 (6.728°), moderate in CC2 (5.923°), and large and negative in CC3 (−6.039°).

In the sagittal plane, CC0 dominates with the largest values across all three parameters: Hip F/E (13.456°), Knee F/E (8.734°), and Ankle DF/PF (10.965°). CC1 and CC2 show moderate, positive values across knee (5.020° and 5.344°) and ankle (6.943° and 5.414°), while Hip F/E in CC1 is near zero (−0.148°) and in CC2 remains small (1.295°). CC3 presents negative values across all sagittal parameters (Hip F/E = −5.330°, Knee F/E = −7.762°, Ankle DF/PF = −4.179°), confirming a response direction opposite to all other clusters.

4.2.4 FoSECTL condition

Table 4.8 Two Legs with Eyes Closed on a Foam Surface

Temporal Formats	**No. of parameters**	**Best Algorithm**	**Outlier Threshold**	**Best *k***	**Evaluation Score**		
					SC	***CH***	***DB***
non-correlated D5I	54	BIRCH/ H-Clust	0.05	4	0.387	30.562	0.729
correlated D5I	25	K-mean	0.05	3	0.385	30.887	0.800
non-correlated S5A	54	H-Clust	0.05	3	0.336	23.316	0.949
correlated S5A	14	K-mean	0.05	3	0.346	27.696	0.956
OTM	9	K-mean	0.05	4	**0.416**	**33.812**	**0.720**

Table 4.8 shows the experimental results of the two legs standing with eyes closed on the foam surface full result can be seen on appendix A Table A4. There were five district temporal formats with and without the correlation execution; which are non-correlated D5I, correlated D5I, noncorrelated S5A, correlated S5A, and TM. The non-correlated S5A yielded the best result on Silhouette Coefficient as 0.416, Calinski-Harabasz as 33.812 and Davies-Bouldin Index as 0.720.the best result in TM type.

Table 4.9 Median Joint of Tri-planar Kinematics by Cluster of FOSECTL

	Frontal plane			Transverse plane			Sagittal plane		
Cluster	**Hip Ab/Ad**	**Knee Ab/Ad**	**Ankle Ab/Ad**	**Hip IR/ER**	**Knee IR/ER**	**Ankle IR/ER**	**Hip F/E**	**Knee F/E**	**Ankle DF/PF**
CD0	(-) 3.911	(-) 0.397	1.143	(-) 0.04	(-) 1.934	4.524	5.201	(-) 0.427	9.818
CD1	(-) 1.366	(-) 0.106	7.078	3.49	0.593	(-) 1.310	1.885	(-) 4.133	4.533
CD2	(-) 2.856	1.195	10.312	8.75	(-) 0.430	0.305	8.178	8.285	10.789
CD3	(-) 19.412	11.448	5.381	(-) 25.63	(-) 1.986	20.322	(-) 2.173	38.895	17.608

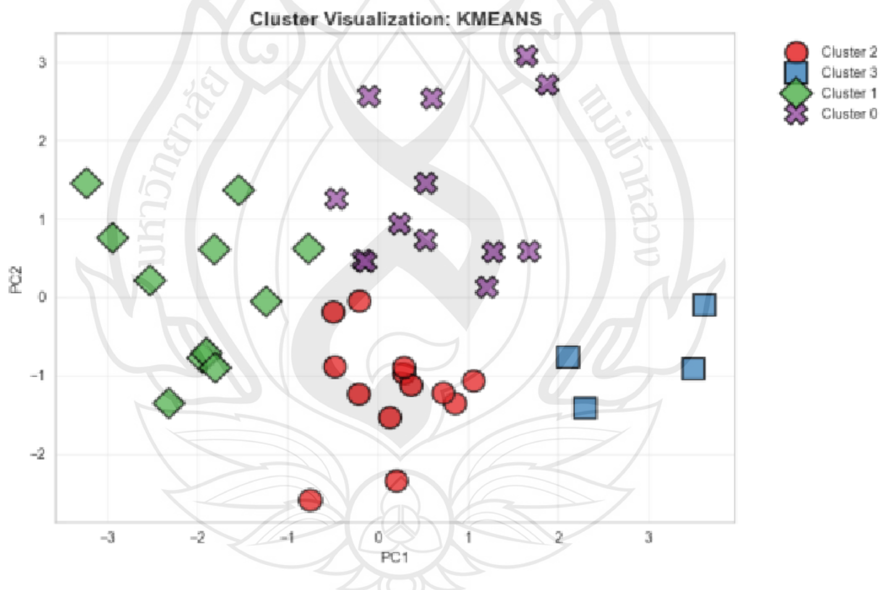

Figure 4.11 Four Clusters of FoSECTL testing from the K-mean algorithm with k=4

The cluster separation observed in Table 4.9 can be substantiated by examining Ankle Dorsiflexion/Plantarflexion (Ankle DP) and Hip Flexion/Extension (Hip FE), both of which show marked differences across clusters on different planar of kinematics using mathematical metrics.

Ankle DP ranges from 4.533° (C1) to 17.608° (C3) — nearly a fourfold difference. C1 shows the lowest ankle dorsiflexion (4.533°), indicating minimal ankle joint excursion, while C0 and C2 show comparable, moderate values (9.818° and 10.789°). C3 reaches 17.608°, approximately 1.6 times higher than C2 and nearly 4 times higher than C1, indicating substantially greater ankle involvement during the response.

Hip FE further differentiates the clusters: C2 shows the highest hip flexion (8.178°), C0 an intermediate value (5.201°), and C1 the lowest positive value (1.885°). C3 is the only cluster with a negative value (-2.173°), indicating hip extension rather than flexion — moving in the opposite direction from the other three clusters at this joint.

Together, these two parameters alone produce four distinct profiles: C1 (low Ankle DP, low Hip FE) reflects a conservative, low-amplitude response; C0 (moderate Ankle DP, moderate Hip FE) reflects a typical ankle-led strategy; C2 (moderate-high Ankle DP, highest Hip FE) reflects greater hip involvement combined with ankle stabilization; and C3 (highest Ankle DP, only negative Hip FE) reflects a divergent strategy combining hip extension with pronounced ankle dorsiflexion. This divergence in C3 is further reinforced by its Knee FE value (38.895) nearly five times higher than the next-highest cluster (C2 = 8.285°) confirming its classification as a distinct, extreme compensatory pattern.

Analysis of Table 4.9 reveals four distinct postural control patterns using a tri-planar kinematic analysis across the frontal, transverse, and sagittal planes.

In the frontal plane, Hip Ab/Ad is negative across all clusters (CD0 = −3.911°, CD1 = −1.366°, CD2 = −2.856°, CD3 = −19.412°), with CD3 showing a markedly larger adduction magnitude — approximately 5–14 times greater than CD0–CD2. Knee Ab/Ad is near zero in CD0 (−0.397°) and CD1 (−0.106°), moderate and positive in CD2 (1.195°), and largest in CD3 (11.448°). Ankle Ab/Ad follows a different pattern: CD2 shows the largest positive value (10.312°), followed by CD1 (7.078°) and CD3 (5.381°), while CD0 remains the lowest (1.143°).

In the transverse plane, Hip IR/ER most clearly differentiates the clusters: CD2 shows the largest internal rotation (8.75°), CD1 shows moderate internal rotation (3.49°), CD0 is near neutral (−0.04°), and CD3 shows by far the largest external rotation

(−25.63), a difference of more than 34° from CD2. Knee IR/ER is small across CD0–CD2 (−1.934° to 0.593°), while CD3 reaches −1.986°, remaining comparatively modest. Ankle IR/ER shows CD0 as the largest positive (4.524°), CD2 near neutral (0.305°), CD1 slightly negative (−1.310°), and CD3 the largest value in the table (20.322°).

In the sagittal plane, the most clinically striking finding is Knee F/E in CD3 (38.895) nearly five times higher than the next-highest cluster (CD2 = 8.285°) and in the opposite direction from CD0 (−0.427°) and CD1 (−4.133°). Hip F/E further differentiates: CD2 shows the highest flexion (8.178°), followed by CD0 (5.201°) and CD1 (1.885°), while CD3 is the only cluster in extension (−2.173°). Ankle DF/PF follows an ascending gradient: CD1 (4.533°) → CD0 (9.818°) → CD2 (10.789°) → CD3 (17.608°).

4.2.5 Balance Strategy Comparison

Table 4.10 Comparison of Balance Strategies

Experiment	Best Algorithms	Best *k*	Best Features	Balance Strategy	Highest Balance Strategy	Population Cluster	N in Cluster
FiSEOTL	BIRCH	4	correlated S5A	Mixed Strategy (HipAnkle)	Knee In/Ex, KneeFle/Ext, Ankle Ab/Ad, Ankle In/Ex, Ankle Dor/Pla	Cluster 0	16, m=6,fm=10
FiSECTL	Spectral	3	correlated D5I	Ankle Strategy	Knee Fle/Ext	Cluster 1	26, m=11,fm=15
FoSEOTL	H-Clust	4	correlated D5I	Ankle Strategy	Ankle Dor/Pla, Hip Fle/Ext	Cluster 2	17, m=9,fm=8
FoSECTL	K-Mean	4	TM	Mix Strategy (Hip,Knee, Ankle)	Ankle Dor/Pla ,Hip Fle/Ext	Cluster 2	17, m=7,fm=10

From Table 4.10, testing four different strategies shows that FiSEOTL, with the majority of the population in cluster 0, uses the Mixed Strategy (Hip-Ankle); FiSECTL, with the majority of the population in cluster 1, and FoSEOTL, with the majority in cluster 2, primarily use the Ankle Strategy; and FoSECTL, with the majority in cluster 2, uses the Mixed Strategy (Hip, Knee, Ankle).

4.3 Summary

Ultimately, Phase 1 defines the classification criteria for balance capability (Good, Slightly Unbalanced, and Poor) based on statistical dispersion and raw angle stability. However, while Phase 1 successfully demonstrated that clustering of lower-limb joint angles can objectively distinguish balance quality groups, it also exposed a key limitation: the three-cluster outcome reveals *how well* an individual balances, but not *how* they achieve it. The macro-level groupings produced by K-Means offered no insight into which specific joint coordination patterns ankle-dominant, hip-dominant, or mixed were responsible for each classification. This gap motivated Phase 2.

Critically, Phase 1 established two methodological foundations that were directly carried forward to phase 2. In phase 1, the use of lower-limb joint angles (hip, knee, and ankle) as the core kinematic features for balance characterization is revealed, and in phase 2, the adoption of a validation on unsupervised clustering with Silhouette Score evaluation is a viable and objective alternative to clinician observation.

Therefore, Phase 2 adopts both principles and extends them to a pediatric population, where balance strategies are more nuanced and harder to classify through subjective observation. Rather than classifying balance quality, Phase 2 acts as the explanatory module that deconstructs those macro classifications by looking at the specific combinations of individual joint rotations (Hip, Knee, and Ankle) pivots that children utilize across different sensory difficulty thresholds of the m-CTSIB to maintain postural stability.

CHAPTER 5

CONCLUSION

5.1 Reactive Balance Strategy Identification

This study developed an objective, data-driven framework for identifying balance strategies from motion capture data using unsupervised machine learning, structured into two sequential phases.

In Phase 1, joint angles at the ankle, knee, and hip were computed from the KINECAL adult dataset using the Law of Cosines, and three clustering algorithms were applied: Agglomerative Hierarchical, Gaussian Mixture Model, and K-Means. The Elbow Method confirmed k=3 as optimal, with K-Means achieving the best Silhouette Score of 0.443. Three postural archetypes were identified: Group 1 (Good Balance) with tight, consistent strategy use; Group 2 (Slight Unbalance) with moderate dispersion and single-strategy reliance; and Group 3 (Poor Balance) with high dispersion and frequent use of multiple compensatory strategies. This confirmed that unsupervised clustering can objectively differentiate balance quality from kinematic data without pre-assigned labels.

In Phase 2, the framework was extended to 44 children aged 7 to 13 years-old performing the m-CTSIB under four sensory conditions using the Xsens 17-sensor IMU system, producing 316,800 data frames. Four algorithms were applied across five temporal feature configurations per condition. The best results were: BIRCH/correlated S5A/k=4 for FiSEOTL (SC=0.420); Spectral/correlated D5I/k=3 for FiSECTL (SC=0.548); H-Clust/correlated D5I/k=4 for FoSEOTL (SC=0.404); and K-Means/OTM/k=4 for FoSECTL (SC=0.416). Four pediatric archetypes were identified: Ankle Strategy, Mixed Hip-Ankle Strategy, Mixed Hip-Knee-Ankle Strategy, and a rare Stiffening Strategy — a joint-locking emergency response observed in one child under FoSECTL that is completely invisible through standard clinical observation.

Together, both phases demonstrate that motion capture combined with unsupervised clustering reveals objective balance strategy patterns — including hidden and mixed archetypes — that traditional observation-based assessment cannot detect.

5.2 Limitations

Although this study produced meaningful results, several limitations should be acknowledged.

In Phase 1, the KINECAL dataset was collected using a Microsoft Kinect system, which has lower spatial accuracy compared to laboratory-grade optical systems. The dataset also contains adult participants only, limiting the generalizability of the Phase 1 archetypes to other populations.

In Phase 2, the sample size of 44 children is relatively small for broad clinical conclusions, and the narrow age range of 7 to 13 years-old may not represent the full developmental spectrum of pediatric balance. All data were also collected under controlled laboratory conditions using static two-leg standing, which may not fully reflect real-world balance demands.

The Stiffening Strategy was observed in only one participant, and its clinical meaning cannot be confirmed from a single case. Further investigation into a larger sample is needed.

Another limitation of this study concerns the relationship between sample size and feature dimensionality. While the original feature set per joint-DoF combination was relatively compact, the construction of time-window-based features (5s, 10s, 15s, 20s, 25s, and 30s) expanded the feature space to 54 dimensions per condition, while the sample size remained at 45 participants. This relatively low sample-to-feature ratio may affect the reliability of distance-based clustering algorithms, as pairwise distances tend to become less discriminative in high-dimensional spaces. Consequently, the identified archetypes should be interpreted as preliminary patterns rather than definitive, generalizable subgroups, and future work should consider dimensionality reduction techniques (e.g., PCA) or larger sample sizes to validate these findings.

A further limitation of this study is the absence of expert-based validation of the identified cluster archetypes. Ideally, the clustering results would be cross-checked against classifications made by clinical experts (e.g., physiotherapists) through visual inspection of motion capture recordings. However, this form of validation requires each expert to review video recordings of every trial and manually annotate the postural strategy employed by each participant—a process that is highly time-consuming given the number of participants, conditions, and trials involved in this study. In addition, manual visual classification of postural strategies is inherently subjective, and establishing reliable ground-truth labels would require multiple expert raters to assess inter-rater agreement, further increasing the time and resource demands beyond the scope of this study. Future work should incorporate a structured validation protocol involving multiple clinical experts to assess the agreement between data-driven cluster archetypes and expert-judged postural strategies.

Finally, the clustering results in both phases are descriptive, not diagnostic. Translating these archetypes into standardized clinical tools would require validation by qualified healthcare professionals and integration with longitudinal outcome data.

5.3 Future Works

Although this study successfully identified distinct balance strategy archetypes in both adults and children, several directions remain open for future research.

The most important next step is to integrate the descriptive archetypes identified in both phases with expert-labeled longitudinal clinical datasets, in order to develop a supervised classification model capable of assigning a balance strategy profile to a new individual automatically — making the framework viable for standardized clinical use.

Future work should also expand the pediatric cohort to include a larger and more diverse sample, covering a wider age range and populations with specific clinical conditions such as Developmental Coordination Disorder (DCD), to validate the identified archetypes across different developmental stages.

This study focused on static two-leg standing only. Extending the framework to dynamic balance tasks — such as single-leg standing or walking — would provide a more complete picture of real-world postural control.

Finally, reducing the sensor requirement from 17 to a smaller number of strategically placed IMUs, while maintaining classification accuracy, would significantly improve the accessibility and practicality of the framework in resource-limited clinical environments.

5.4 List of Publication

Lapawong, W., Uttama, S., Rueangsirarak, W., Temdee, P., Hu, S., & Aslam, N. (2025). Understanding human balance strategies through clustering of motion analysis data. In *2025 ECTI DAMT & NCON* (pp. 400–405). IEEE. Nan, Thailand. https://doi.org/10.1109/ECTIDAMTNCON64748.2025.10962119

Lapawong, W., Uttama, S., Yingyongsaksri, S., Kunritt, J., & Rueangsirarak, W. (in press). Identifying children's hidden balance strategy in mCTSIB using clustering techniques. In *Proceedings of the 23rd International Joint Conference on Computer Science and Software Engineering (JCSSE 2026).* Bangkok, Thailand.

REFERENCES

Al-Amri, M., Nicholas, K., Button, K., Sparkes, V., Sheeran, L., & Davies, J. L. (2018). Inertial measurement units for clinical movement analysis: Reliability and concurrent validity. *Sensors*, *18*(3), Article 719. https://doi.org/10.3390/s18030719

Alhafis Hashim, M. E., Wan Mustafa, W. A., Prameswari, N. S., Md Ghani, M., & Hanafi, H. F. (2024). Revolutionizing virtual reality with generative AI: An in-depth review. *Journal of Advanced Research in Computing and Applications*, *30*(1), 19–30. https://doi.org/10.37934/arca.30.1.1930

Atkeson, C. G., & Stephens, B. (2007). Multiple balance strategies from one optimization criterion. In *2007 7th IEEE-RAS International Conference on Humanoid Robots* (pp. 57–64). IEEE. https://doi.org/10.1109/ICHR.2007.4813848

Barry, E., Galvin, R., Keogh, C., Horgan, F., & Fahey, T. (2014). Is the Timed Up and Go test a useful predictor of risk of falls in community dwelling older adults: A systematic review and meta-analysis. *BMC Geriatrics*, *14*(1), 14. https://doi.org/10.1186/1471-2318-14-14

Berg, K. O., Wood-Dauphinee, S. L., Williams, J. I., & Maki, B. (1992). Measuring balance in the elderly: Validation of an instrument. *Canadian Journal of Public Health*, *83*(S2), S7–S11.

Bishop, C. M. (2006). *Pattern Recognition and Machine Learning*. Springer.

Blenkinsop, G. M., Pain, M. T. G., & Hiley, M. J. (2017). Balance control strategies during perturbed and unperturbed balance in standing and handstand. *Royal Society Open Science*, *4*(7), Article 161018. https://doi.org/10.1098/rsos.161018

CanChild. (n.d.). *Developmental coordination disorder*. Dyspraxia Foundation. Retrieved April 14, 2026, from https://dyspraxiafoundation.co.uk/dyspraxia-children/

CanChild. (n.d.). *Developmental coordination disorder*. Retrieved April 14, 2026, from https://canchild.ca/diagnoses/developmental-coordination-disorder/

Cavallo, A., Koul, A., Ansuini, C., Capozzi, F., & Becchio, C. (2016). Decoding intentions from movement kinematics. *Scientific Reports*, *6*, Article 37036. https://doi.org/10.1038/srep37036

Cuisinier, R., Olivier, I., Vaugoyeau, M., Nougier, V., & Assaiante, C. (2011). Reweighting of sensory inputs to control quiet standing in children from 7 to 11 and in adults. *PLoS ONE*, *6*(5), Article e19697. https://doi.org/10.1371/journal.pone.0019697

Di Raimondo, G., Vanwanseele, B., van der Have, A., Emmerzaal, J., Willems, M., Killen, B. A., & Jonkers, I. (2022). Inertial sensor-to-segment calibration for accurate 3D joint angle calculation for use in OpenSim. *Sensors*, *22*(9), Article 3259. https://doi.org/10.3390/s22093259

Duncan, P. W., Weiner, D. K., Chandler, J., & Studenski, S. (1990). Functional reach: A new clinical measure of balance. *Journal of Gerontology*, *45*(6), M192–M197. https://doi.org/10.1093/geronj/45.6.M192

Eltoukhy, M., Kuenze, C., Oh, J., Wooten, S., & Signorile, J. (2017). Kinect-based assessment of lower limb kinematics and dynamic postural control during the star excursion balance test. *Gait & Posture*, *58*, 421–427. https://doi.org/10.1016/j.gaitpost.2017.09.010

GeeksforGeeks. (n.d.). *Naive Bayes classifiers.* Retrieved April 12, 2026, from https://www.geeksforgeeks.org/naive-bayes-classifiers/

Ghoraani, B. (2024). Objective estimation of m-CTSIB balance test scores using wearable sensors and machine learning. *Frontiers in Digital Health*, *6*, 1366176. https://doi.org/10.3389/fdgth.2024.1366176

Gul, J. Z., Cheema, M. O., Mohy Ud Din, Z., Khan, M., Kim, W. Y., & Rehman, M. M. (2024). Machine learning-based classification of body imbalance and its intensity using electromyogram and ground reaction force in immersive environments. *Applied Sciences*, *14*(18), Article 8209. https://doi.org/10.3390/app14188209

Haas, B., Clarke, E., Elver, L., Gowman, E., Mortimer, E., & Byrd, E. (2017). The reliability and validity of the L-test in people with Parkinson's disease. *Physiotherapy*, *103*(1), 70–77.

Halilaj, E., Rajagopal, A., Fiterau, M., Hicks, J. L., Hastie, T. J., & Delp, S. L. (2018). Machine learning in human movement biomechanics: Best practices, common pitfalls, and new opportunities. *Journal of Biomechanics, 81*, 1–11.

Halvorson, R. T., Castillo, F. T., Ahamed, F., Khattab, K., Scheffler, A., Matthew, P. R., et al. (2022). Point-of-care motion capture and biomechanical assessment improve clinical utility of dynamic balance testing for lower extremity osteoarthritis. *PLOS Digital Health, 1*(7), Article e0000068. https://doi.org/10.1371/journal.pdig.0000068

Harris, S. R., Mickelson, E. C. R., & Zwicker, J. G. (2015). Diagnosis and management of developmental coordination disorder. *CMAJ*, *187*(9), 659–665. https://doi.org/10.1503/cmaj.140994

Hoadley, J. F., Kranz, A. M., Jones, S. S., & Sorbero, M. E. (2018). Applying machine learning algorithms to segment high-cost patient populations. *Journal of General Internal Medicine*, *33*(12), 2087–2094. https://doi.org/10.1007/s11606-018-4669-z

Horak, F. B. (2006). Postural orientation and equilibrium: What do we need to know about neural control of balance to prevent falls? *Age and Ageing*, *35*(Suppl 2), ii7–ii11. https://doi.org/10.1093/ageing/afl077

Horak, F. B., & Nashner, L. M. (1986). Central programming of postural movements: Adaptation to altered support-surface configurations. *Journal of Neurophysiology*, 55(6), 1369–1381. https://doi.org/10.1152/jn.1986.55.6.1369

Jonsson, E., Henriksson, M., & Hirschfeld, H. (2003). Does the functional reach test reflect stability limits in elderly people? *Journal of Rehabilitation Medicine*, *35*(1), 26–30. https://doi.org/10.1080/16501970306099

Keshmiri, A., & Etemad, A. (2024). A comprehensive survey on markerless motion capture: Approaches and applications in fall risk assessment. *Sensors*, *24*(14), Article 4593. https://doi.org/10.3390/s24144593

Maudsley-Barton, S., & Yap, M. H. (2024). Objective falls risk assessment using markerless motion capture and representational machine learning. *Sensors*, *24*(14), Article 4593. https://doi.org/10.3390/s24144593

Mayer, J., Jose, R., Bekbolatova, M., Coletti, C., Devine, T., & Toma, M. (2024). Enhancing patient safety through integrated sensor technology and machine learning for bed-based patient movement detection in inpatient care. *Artificial Intelligence in Health*, *1*, Article 2790. https://doi.org/10.36922/aih.2790

McManus, K., Greene, B. R., Ader, L. G. M., & Caulfield, B. (2022). Development of data-driven metrics for balance impairment and fall risk assessment in older adults. *IEEE Transactions on Biomedical Engineering, 69*(7), 2324–2332.

Miyazawa, Y., Nomoto, H., Sato, M., Shiga, H., Sugawara, H., Nakamura, J., & Cho, K. Y. (2020). Identification of two novel subgroups in patients with diabetes through cluster analysis. *Journal of Diabetes Investigation*, *11*(6), 1542–1551. https://doi.org/10.1111/jdi.13289

Movella. (n.d.). *MVN Awinda.* Retrieved April 12, 2026, from https://www.movella.com/products/motion-capture

Museck, I. J., Brinton, D. L., & Dean, J. C. (2024). The use of wearable sensors and machine learning methods to estimate biomechanical characteristics during standing posture or locomotion: A systematic review. *Sensors*, *24*(22), Article 7280. https://doi.org/10.3390/s24227280

Neptune, R. R., & Vistamehr, A. (2019). Dynamic balance during human movement: Measurement and control mechanisms. *Journal of Biomechanical Engineering*, *141*(7), 070801. https://doi.org/10.1115/1.4042170

Nijmeijer, E. M., Heuvelmans, P., Bolt, R., Gokeler, A., Otten, E., & Benjaminse, A. (2023). Concurrent validation of the Xsens IMU system of lower-body kinematics in jump-landing and change-of-direction tasks. *Journal of Biomechanics, 154*, Article 111637. https://doi.org/10.1016/j.jbiomech.2023.111637

Osness, E., Isley, S., Bertrand, J., Dennett, L., Bates, J., Van Decker, N., et al. (2025). Markerless motion capture parameters associated with fall risk or frailty: *A scoping review. Sensors, 25(*18), Article 5741. https://doi.org/10.3390/s25185741

PhysioPedia. (n.d.). *Anticipatory adjustments: Balance intervention strategies. PhysioPedia.* Retrieved April 14, 2026 from https://www.physio-pedia.com/Anticipatory_Adjustments:_Balance_Intervention_Strategies

PhysioPedia. (n.d.). *Balance assessment.* PhysioPedia. Retrieved April 14, 2026 from https://www.physio-pedia.com/Balance_Assessment

PhysioPedia. (n.d.). *Timed Up and Go Test (TUG). PhysioPedia.* Retrieved April 14, 2026, from https://www.physio-pedia.com/Timed_Up_and_Go_Test_(TUG)

Pirker, W., & Katzenschlager, R. (2017). Gait disorders in adults and the elderly. *Wiener Klinische Wochenschrift*, *129*(3–4), 81–95. https://doi.org/10.1007/s00508-016-1096-4

Rhode Island Department of Health. (n.d.). *Childhood falls*. Retrieved April 14, 2026, from https://health.ri.gov/injury-prevention/childhood-falls

Roshdibenam, V., Jogerst, G. J., Butler, N. R., & Baek, S. (2021). Machine learning prediction of fall risk in older adults using Timed Up and Go test kinematics. *Sensors*, *21*(10), Article 3481. https://doi.org/10.3390/s21103481

Russell, S. J., & Norvig, P. (2021). *Artificial Intelligence: A Modern Approach* (4th ed.). Pearson.

Sang, Y., Matsushita, K., Grams, M. E., Chang, A. R., Ballew, S. H., Woodward, M., & Coresh, J. (2022). Characterization of data-driven clusters in diabetes-free adults and their association with risk of type 2 diabetes and cardiovascular disease. *BMC Medicine*, *20*, Article 307. https://doi.org/10.1186/s12916-022-02506-6

Scataglini, S., Abts, E., Van Bocxlaer, C., Van den Bussche, M., Meletani, S., & Truijen, S. (2024). Accuracy, validity, and reliability of markerless camera-based 3D motion capture systems versus marker-based 3D motion capture systems in gait analysis: *A systematic review and meta-analysis. Sensors, 24*(11), Article 3686. https://doi.org/10.3390/s24113686

Secure Safety Solutions. (2020, December 1). *CDC fall statistics & nursing home falls*. https://www.securesafetysolutions.com/cdc-fallstatistics/

Sensing Future. (n.d.). *Modified Clinical Test of Sensory Interaction in Balance (m-CTSIB): How to perform and interpret the results.* Sensing Future. Retrieved April 12, 2026, from https://sensingfuture.com/blog/modified-clinical-test-of-sensory-interaction-in-balance-m-CTSIB-how-to-perform-and-interpret-the-results/

Shen, K., Chemori, A., & Hayashibe, M. (2020). Human-like balance recovery based on numerical model predictive control strategy. *IEEE Access*, *8*, 103212–103221. https://doi.org/10.1109/ACCESS.2020.2995104

Shumway-Cook, A., & Horak, F. B. (1986). Assessing the influence of sensory interaction on balance: Suggestions from the field. *Physical Therapy*, *66*(10), 1548–1550. https://doi.org/10.1093/ptj/66.10.1548

Shumway-Cook, A., & Woollacott, M. H. (2017). *Motor Control: Translating Research into Clinical Practice* (5th ed.). Wolters Kluwer.

Smeenk, R. (2014, March 11). *Kinect V1 and Kinect V2 fields of view compared*. https://smeenk.com/kinect-field-of-view-comparison/

Tamplain, P., Miller, H. L., Peavy, D., Cermak, S., Williams, J., & Licari, M. (2024). The impact for DCD – USA study: The current state of developmental coordination disorder (DCD) in the United States of America. *Research in Developmental Disabilities*, *145*, 104658. https://doi.org/10.1016/j.ridd.2023.104658

Westcott, S. L., Lowes, L. P., & Richardson, P. K. (1997). Evaluation of postural stability in children: Current theories and assessment tools. *Physical Therapy*, *77*(6), 629–645. https://doi.org/10.1093/ptj/77.6.629

Winter, D. A. (1995). Human balance and posture control during standing and walking. *Gait & Posture*, *3*(4), 193–214.

Wirz, M., Müller, R., & Bastiaenen, C. (2010). Falls in persons with spinal cord injury: Validity and reliability of the Berg Balance Scale. *Neurorehabilitation and Neural Repair*, *24*(1), 70–77. https://doi.org/10.1177/1545968309341059

World Health Organization. (2007). *WHO global report on falls prevention in older age.* https://www.who.int/publications/i/item/9789241563536

World Health Organization. (2022, September 27). *Musculoskeletal conditions.* https://www.who.int/news-room/fact-sheets/detail/musculoskeletal-conditio

Wu, G., Siegler, S., Allard, P., Kirtley, C., Leardini, A., Rosenbaum, D., et al. (2002). ISB recommendation on definitions of joint coordinate system of various joints for the reporting of human joint motion—Part I: ankle, hip, and spine. *Journal of Biomechanics, 35*(4), 543–548. https://doi.org/10.1016/S0021-9290(01)00222-6

Xiong, S. (2017). Accuracy of base of support using an inertial sensor based motion capture system. *Sensors*, *17*(9), 2091. https://doi.org/10.3390/s17092091

Zago, M., Rozin Kleiner, A. F., & Federolf, P. A. (2021). Editorial: Machine learning approaches to human movement analysis. *Frontiers in Bioengineering and Biotechnology*, *9*, Article 635435. https://doi.org/10.3389/fbioe.2021.635435

Zwicker, J. G., Missiuna, C., Harris, S. R., & Boyd, L. A. (2012). Developmental coordination disorder: A review and update. *European Journal of Paediatric Neurology*, *16*(6), 573–581. https://doi.org/10.1016/j.ejpn.2012.05.005

APPENDIX A

COMPELETE CLUSTERING EVALUATION RESULTS FOR M-CTSIB CONDITIONS ACROSS ALL TEMPORAL FORMATS AND ALGORITHMS

Table A1 Firm Surface, Eyes Open, Two Legs-standing (FiSEOTL)

Condition	Outlier Ratio	K clusters	Algorithm	Silhouette	Calinski-Harabasz	Davies-Bouldin
No correction each 5s	0.1	3	K-means	0.3258	18.7226	1.0261
			Spectral (SC)	0.3352	15.6046	0.6652
			BIRCH	0.3104	22.0656	0.9529
			H-Clust	0.3615	26.5753	0.863
Correction each 5s	0.1	4	K-means	0.3638	27.7109	0.8339
			Spectral (SC)	0.36	26.2108	0.8681
			BIRCH	0.3217	22.3903	0.727
			H-Clust	0.3678	26.0301	0.8276
No correction avg 5s	0.1	4	K-means	0.3174	22.7942	0.8575
			Spectral (SC)	0.2616	9.0309	1.0578
			BIRCH	0.3151	22.9242	0.9337
			H-Clust	0.3125	22.2865	0.9819
Correction avg 5s	0.05	4	K-means	0.3955	29.8493	0.6947
			BIRCH	**0.4201**	**29.6771**	**0.5779**
			H-Clust	**0.4201**	**29.6771**	**0.5779**
			Spectral (SC)	0.3098	20.4005	0.6945
Mean	0.05	4	K-means	0.3273	22.1521	0.8744
			Spectral (SC)	0.3419	18.6063	0.7742
			BIRCH	0.3784	26.5999	0.6432
			H-Clust	0.3707	27.1362	0.6253

Table A2 Firm Surface, Eyes Closed, Two Legs-standing (FiSECTL)

Condition	Outlier Ratio	K clusters	Algorithm	Silhouette	Calinski-Harabasz	Davies-Bouldin
No correlation (each 5s)	0.08	4	sc (Spectral Clustering)	0.3831	20.3557	0.9803
			kmeans	0.3402	30.2836	0.9368
			hclust	0.3061	24.8131	0.8499
			birch	0.2928	25.878	0.9724
correlation (each 5s)	0.05	3	sc (Spectral Clustering)	0.5485	22.7585	0.4477
			birch	0.4293	26.5495	0.7862
			kmeans	0.3944	30.1184	0.8104
			hclust	0.3669	29.2909	0.8477
No Correction (avg 5s)	0.05	4	birch / hclust	0.3833	26.7704	0.6859
			kmeans	0.3824	27.4852	0.6511
correction			sc	0.2918	14.7791	0.9274
(avg 5s)			kmeans	0.4004	31.9623	0.7862
correlation	0.05	4	sc	0.3912	24.9553	0.6364
avg 5s			hclust	0.381	26.948	0.8161
Mean			birch	0.3521	25.1056	0.7882
			sc (Spectral Clustering)	0.446	21.9132	0.6138
Mean	0.05	3	kmeans	0.4409	25.3025	0.6386
			hclust	0.4158	28.1037	0.8306
			birch	0.4138	27.7734	0.8085
			sc (Spectral Clustering)	0.3831	20.3557	0.9803

Table A3 Foam Surface, Eyes Open, Two Legs-standing (FoSEOTL)

Condition	Outlier Ratio	K clusters	Algorithm	Silhouette	Calinski-Harabasz	Davies-Bouldin
No correlation (each 5s)	0.05	4	H-Clust	0.3349	25.8414	0.9562
			BIRCH	0.3186	24.2046	0.918
			K-means	0.2526	23.3621	1.0282
			Spectral (SC)	0.2837	15.9893	0.8214
correlation (each 5s)	0.05	4	H-Clust	0.4041	28.9403	0.6629
			BIRCH	0.3912	31.2368	0.7792
			Spectral (SC)	0.3762	27.2216	0.8308
			K-means	0.3507	25.2635	0.903
No correlation (avg 5s)	0.05	4	K-means	0.3344	26.9885	0.9236
			H-Clust	0.3323	25.527	0.9163
			BIRCH	0.3304	24.1611	0.9588
			Spectral (SC)	0.2036	13.0643	0.8575
correlation (avg 5s)	0.05	4	BIRCH	0.4292	21.151	0.7199
			Spectral (SC)	0.4115	22.3529	0.9206
			K-means	0.3669	22.3629	0.7697
			H-Clust	0.3483	21.4196	0.841
Mean	0.05	4	BIRCH	0.4091	21.0367	0.7339
			Spectral (SC)	0.3859	20.2512	0.8549
			K-means	0.3539	15.7161	0.7492
			H-Clust	0.3143	19.8771	1.0039

Table A4 Foam Surface, Eyes Closed, Two Legs-standing (FoSECTL)

Condition	Outlier Ratio	K clusters	Algorithm	Silhouette	Calinski-Harabasz	Davies-Bouldin
No correlation each 5s	0.05	4	**BIRCH**	**0.3867**	**30.5628**	**0.7292**
			H-Clust	**0.3867**	**30.5628**	**0.7292**
			K-means	0.3717	30.5049	0.742
			Spectral (SC)	0.1747	13.5317	0.8948
correlation (each 5s)	0.05	3	**K-means**	**0.3853**	**30.8872**	0.8004
			BIRCH	0.3742	29.5873	0.9165
			H-Clust	0.368	27.5885	0.8412
			Spectral (SC)	0.3039	14.5014	**0.7439**
No correlation avg 5s	0.05	3	**H-Clust**	**0.3363**	**23.3158**	0.9486
			Spectral (SC)	0.3177	21.1123	**0.9278**
			BIRCH	0.3114	22.255	0.9606
			K-means	0.3113	22.5791	0.9495
correlation avg 5s	0.05	3	**K-means**	**0.3457**	**27.6956**	0.956
			H-Clust	0.3252	26.0631	0.9934
			BIRCH	0.3145	25.0792	**0.9388**
			Spectral (SC)	0.3111	23.3067	0.9765
Mean	0.05	4	**K-means**	**0.4164**	**33.8115**	**0.7203**
			H-Clust	0.3954	29.1506	0.7662
			BIRCH	0.3911	31.3507	0.7876
			Spectral (SC)	0.3514	22.7287	0.7393

CURRICULUM VITAE

NAME Werapat Lapawong

EDUCATIONAL BACKGROUND

2021 Bachelor of Science
Information Technology
Mae Fah Luang University

WORK EXPERIENCE

2026-Present Co-Researcher
NSTDA

PUBLICATION

Lapawong, W., Uttama, S., Rueangsirarak, W., Temdee, P., Hu, S., & Aslam, N. (2025). Understanding human balance strategies through clustering of motion analysis data. In *2025 Joint International Conference on Digital Arts, Media and Technology with ECTI Northern Section Conference on Electrical, Electronics, Computer and Telecommunications Engineering (ECTI DAMT & NCON)* (pp. 400–405). IEEE. https://doi.org/10.1109/ECTIDAMTNCON64748.2025.10962119

Thammachokmongkol, P., Lapawong, W., & Rueangsirarak, W. (2025). Evaluating online content accessibility using WCAG 2.1: A case study of university platforms and an e-learning system for students with visual impairments. In *2025 9th International Conference on Information Technology (InCIT)* (pp. 578–583). IEEE. https://doi.org/10.1109/InCIT66780.2025.11276028

Kurubanjerdjit, N., Kirimasthong, K., Nupap, S., Sutthaluang, T., Kloomsilp, C., & Lapawong, W. (2021). The discovery of microRNA–phytochemicals interaction of diseases caused by viruses using ensemble data mining techniques. In *2021 13th International Conference on Information Technology and Electrical Engineering (ICITEE)* (pp. 159–164). IEEE. https://doi.org/10.1109/ICITEE53064.2021.9611939